NASA CONTRACTOR REPORT 166522

Fused Silica Mirror Development for SIRTF

William P. Barnes, Jr.

(NASA-CR-166522) FUSED SILICA MIRRCR DEVELOPMENT FOR SIRTF (Itek Corp.) 90 p HC A05/MF A01 CSCL 03A

N83-35959

Unclas
G3/89 42073

CONTRACT NAS2– 10859
July 1983

NASA

NASA CONTRACTOR REPORT 166522

Fused Silica Mirror Development for SIRTF

William P. Barnes, Jr.
Itek Optical Systems Division
Litton Industries
Lexington, Massachusetts

Prepared for
Ames Research Center
under Contract NAS2-10869

National Aeronautics and
Space Administration

Ames Research Center
Moffett Field, California 94035

Table of Contents

1. Introduction and Summary
2. Statement of Work
3. Telescope Wavefront Error Budget and Test Accuracy
4. Test Arrangement
5. Results - First Cold Cycle
6. Results - Second Cold Cycle
7. Results - Post Test Inspection
8. Discussions and Conclusions
9. Recommendations

Appendix A - Test System Thermal Analyses

Appendix B - Component Verification Tests

Appendix C - Temperature Instrumentation

Appendix D - Interferometric Data Reduction - First Cold Cycle

Appendix E - Interferometric Data Reduction - Second Cold Cycle

1. INTRODUCTION and SUMMARY

The principal purpose of this task was to determine the optical figure changes of a fused silica mirror, mounted in an aluminum structure, at temperatures of 30 kelvins or less. The test arrangement included a tangent flexure mounting and conductive thermal connectors chosen to be viable candidates for a flight-qualified telescope system. The test cycles were successfully executed, and mirror temperatures as low 12.8 kelvins were attained. Unpredicted, but in retrospect not unusual, local figure irregularities were observed. They correlated perfectly with the core configuration of the lightweight mirror. These irregularities are almost certainly a result of thermal flux from the large, warm, observing window. Although the window emittance at wavelengths longer than 5μm had been reduced by a multi-layer metal-dielectric coating, calculations based on its measured reflectance indicate that it is radiating a total of 25 watts into the test chamber.

The worst case mirror surface variations from a true sphere amounted to 0.28 waves rms at a test wavelength of 633nm, or 0.18μm rms. We originally reduced our data on the basis of differencing room temperature and cold mirror interferograms. However, we further discovered that the mirror surface was moving quite rapidly during our observation, and temperature data indicated that large thermal fluxes are present. We believe that any changes which might be ascribed to material property inhomogeneity are engulfed by the thermal gradient deflections which develop in a matter of seconds during the optical observation periods.

The thermal flux boundary conditions of our tests have proven to be much more severe than those expected in the SIRTF operational environment. The value of our tests lies in a demonstration that solutions for conductive cooling and mounting of a fused silica mirror in an aluminum structure for use at 10 kelvins are close at hand, and that the ultimate design of component and telescope system testing facilities for SIRTF will require very close attention to all details of the thermal boundary conditions imposed. Further cryogenic testing of fused silica mirrors, freed from the restrictions and boundary conditions of these tests - an existing mirror fitted into an existing test chamber - appears well recommended.

Some failures of the thermal connectors recommend design refinements and further breadboard testing of such components. More precise experimental characterization of the effect of structure deflections acting through the mount flexures to produce mirror figure changes is desirable.

The mount design appears to have performed as expected, with no evidence of any failure or malfunction. Forces transmitted through the mount as a result of differential expansion between the mirror and mounting ring primarily affect the cylindrical and "tricorn" (2θ and 3θ) mirror deflections. Both absolute values and differences in these deflections remained below 1 wave peak-to-valley (at 633nm) in all cases examined.

2. STATEMENT OF WORK

Paragraph 2.1 and 2.2 are quoted verbatim from the contract document.

2.1 SCOPE AND PURPOSE

The contractor shall provide the personnel, materials, and facilities needed to evaluate the capability of a light-weighted fused silica mirror to meet the following goals:

1. Hold figure at cryogenic temperature
2. Be mounted so that differential expansion effects at cryogenic temperature will not exceed the required figure tolerance.
3. Be cooled to uniform temperatures across the mirror at operating temperature.

The contractor shall provide the demonstration program described herein, using a test mirror selected so that the results can be applied to a 1-meter-class telescope.

2.2 TASKS

The contractor shall perform the following:

2.2.1 Define an optical system that will meet the performance requirements of the Shuttle Infrared Telescope Facility (SIRTF) contained in specification 2-27981 attached. Deviations from specified mirror requirements shall be permissible to take advantage of fused silica capabilities. Derive an overall system optical tolerance budget intended to achieve diffraction-limited performance at 2μm wavelength at 10K temperature, and assign the tightest tolerances that are feasible, within current proven technology, to the primary mirror. Convert this requirement to an rms surface figure error requirement for the mirror. The optical design and the tradeoffs that support its selection shall be reviewed with ARC at or prior to design review.

2.2.2 Show analytically that the selected Itek-Heraeus IR&D mirror can be used to evaluate the capability of a fused silica mirror for use as a SIRTF-size primary mirror, based on the tolerance budget from Task 1.

2.2.3 Design mounts and heat exchange provisions (using conductive and radiative cooling) for the test mirror. The mounts and heat exchange provisions shall be analytically shown to allow the mirror to meet the figure requirements assigned by Task 1, and to be scaleable to SIRTF size.

2.2.4 Modify the test mirror as required. Fabrication of the test mirror shall use proven techniques applicable to SIRTF.

2.2.5 Fabricate the mounts and heat exchange provisions designed in Task 3.

2.2.6 Assemble the mirror and mounts onto an aluminum test fixture representative of the telescope, and make interferograms at a suitable wavelength to ascertain that at room temperature the surface figure error with optical axis horizontal is 0.04μm rms (equivalent to diffraction limit at 2μm).

2.2.7 Using the same test fixture and a comparable test setup the mirror shall be cooled at 30K or below, and interferograms shall be made. The mirror will be cooled as much below 30K as is reasonably achievable, with a goal of 20K. Data taking will start at as low a temperature below 30K as is reasonably achievable for each data taking sequence i.e. start to adjust focus and take interferograms at or below 30K. (Each data taking sequence of focus adjust and interferogram taking is estimated to require 5 to 6 minutes.) The figure changes due to cooling will be determined by comparing the resulting interferograms with the room temperature interferograms. The cycle from room temperature to 30K or less will be repeated once. Mirror temperature uniformity shall be estimated from smoothed temperature-time data at a few mirror locations.

2.2.8 Compare the analytical and test results for predictability of mirror performance. Describe any additional figuring necessary to achieve the required figure at low temperature.

2.3 AMENDMENTS

Two additions to the statement of work, both representing some increase in the scope of the work were issued.

2.3.1 Amendment of February 1982

Upgrade the low temperature thermometry on the fused silica mirror and cooling link to the mechanical cooler by use of silicon diode sensors.

Verify proper operation of the mechanical cooler with the improved thermometers in an offline test prior to initiation of the mirror test sequences.

2.3.2 Amendment of May 1983

The contractor is directed to make and analyze a real-time, video record of test interferometry. A continuous measurement in real time of the optical properties of the Itek/Heraeus fused silica test mirror at cryogenic temperature is needed to evaluate, in at least one case, the transient in optical performance under the thermal load conditions existing in this test.

3. TELESCOPE WAVEFRONT ERROR BUDGET AND TEST ACCURACY

Our tolerance analysis of a nominal 0.85m aperture, f/24 Cassegrain telescope with a central obstruction of 40% linear obscuration, together with some results of our study of the Teal Ruby telescope system then under construction, were used to construct the wavefront error budget shown in Figure 3-1. This budget establishes, on a bottom-up basis, our best current estimate of the errors anticipated in a fused silica SIRTF telescope toleranced for diffraction-limited performance at 2μm. For the primary mirror we have computed an error for a temperature soak from room temperature to 10°K. The value shown assumes no cold null figuring and is based on a scaling of previous cold test results for a 72-in. ULE mirror. Note also that if the mirror has a front-to-back expansion coefficient variation there will be a focus change when subjected to the temperature offset from room temperature to 10K. For a 10^{-8}/K differential expansion we would experience up to 0.2-in. of defocus in the image plane. This is of no consequence to telescope operation since a mean focal position would be established experimentally. Variations about the mean temperature are accommodated in the "differential soak" form.

Axial/radial gradient and mount errors coming from differences in expansion between the mount and the mirror substrate (or differential expansion coefficient effects within the mount proper) were established based on the Teal Ruby analysis.

The axial gradient value of 0.08 wave represents approximately 1/8°C allowable axial gradient on the primary mirror.

Secondary mirror errors have been set at one-third those of the primary based on Teal Ruby experience.

Error sources on the reflected beam from the beam splitter have been established as equivalent to those of the secondary mirror for first-cut budget purposes. The effects on the refracting component are likely to be more severe, but have not been addressed here.

PRELIMINARY SIRTF ERROR BUDGET

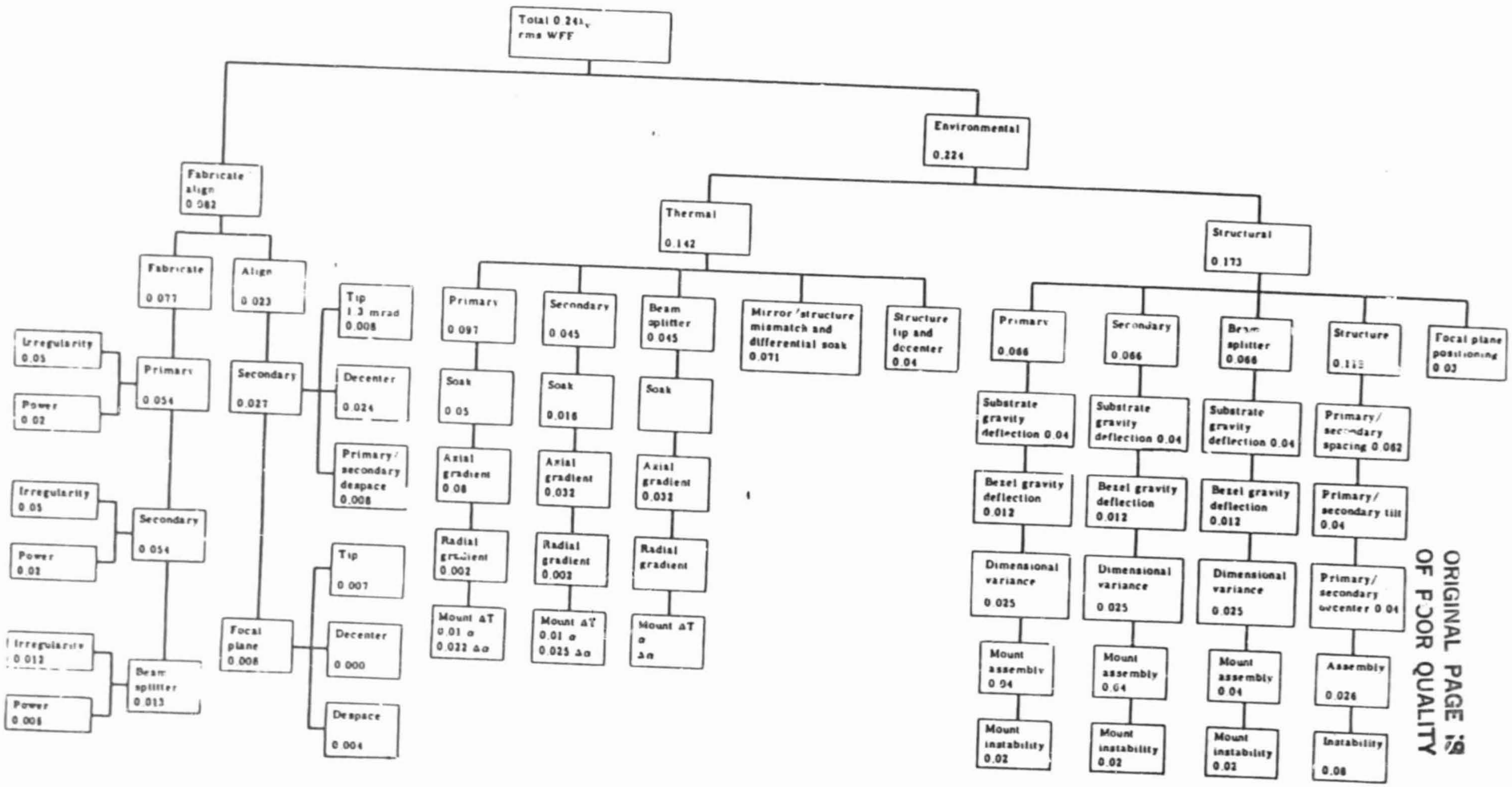

Figure 3-1

Itek Optical Systems

The thermal error source entitled "mirror structure mismatch and differential soak" represents the degree of athermalization of the telescope at its operational cryogenic temperature. Thus although the telescope is focused for operation at 10 K , swings around 10°K coupled with any differential expansion between the mirror and the structure will result in defocus and other wavefront errors. In this error source we have also included the effects of the front-to-back expansion coefficient variations within the mirror structures as cascaded with an estimated ± 5K temperature variation as well as the minor effects of radius changes due to uniform expansion within the mirror substrates.

When one totals all of the error sources associated with the primary mirror, we find an rms wavefront error total of about 0.13λ (to 0.15λ, as a function of gravity deformation). Thus, for our demonstration mirror we planned to detect changes of 0.05 to 0.07 wave of thermo-optically induced inhomogeneity error from room temperature to 10 K out of error totals of 0.15λ rms WFE. Test accuracies of 0.01 to 0.02λ rms were expected.

4. TEST ARRANGEMENT

A critical understanding of the probable performance of fused silica as the SIRTF primary mirror material was determined to require optical surface evaluation of a mirror that is:

1. Moderately lightweight
2. Representative of current fabrication technology
3. Not far different in scale from the expected SIRTF aperture, which may approach 1m.
4. Supported in a structure that simulates an aluminum telescope structure.
5. Tested at a temperature of 30 K or colder.

Itek Optical Systems had already undertaken a joint IR&D effort with Heraeus-Amersil for construction of a 26-in. diameter mirror for evaluation of the combination of Itek's numerically controlled machining of fused silica and the Heraeus-Amersil expertise in arc fusion of silica. In addition, Itek determined that an existing thermal-optical vacuum test chamber, having a liquid nitrogen shroud and a Cryo-Torr Model 20 cryo pump, could be modified for lower-temperature operation and would accommodate the 26-in. mirror. This test chamber has a high-quality BK-7 observation window with a 34-in. diameter clear aperture. With the cooperation of Heraeus-Amersil, and the agreement of Itek management that the chamber modification represented a prudent capital investment for future needs, we were able to structure the total evaluation effort.

The design and construction of an additional, helium cryostat-cooled, thermal shroud for the test chamber presented some practical problems in fitting it and the mirror mounting details between the 26.5-in. major mirror diameter and the 35-in. inner diameter of the existing liquid nitrogen-cooled shroud. At the same time, we had to minimize parasitic heat leaks to the shroud and mirror and ensure good thermal contact between all parts of the shroud and to the mirror. The achievement of practical cool down times, and the reduction of thermal gradients when stable test conditions were desired, necessitated careful analysis of all the thermal boundary conditions expected.

For example, we found that the most critical boundary condition for the optical tests was not direct radiation from the window to the mirror, but radiation to the inner surface of the shroud then conduction through the shroud and mirror thermal conductors to the <u>rear</u> surface of the mirror. Subsequent consideration also indicates that the energy reflected to the open annulus left between mirror and shroud, then absorbed at the uncoated side and rear surfaces of the mirror is an additional perturbation. Multiple reflections in the mirror-window optical cavity also contribute to this transfer path.

Conductive connections to the mirror are needed because radiative cooling of the mirror mass to temperatures much below 100K leads to impractically long cooling times. At 30K, black body radiation to a 0K sink requires 15 hours to reduce the temperature of a 1cm thickness of fused silica by 1K.

A final critical item in the test arrangement was the detailed design of the mechanical connections between the mirror and the aluminum auxiliary shroud used to simulate the ultimate SIRTF telescope structure. Here we copied from the tangential flexure leaf, flexural pivot connection used in our Teal Ruby telescope but using aluminum throughout in place of Invar. We fortunately included a breadboard test of this substitution. Modification and retesting, as detailed in Appendix 2, indicates that the combination of an Invar pivot and an aluminum leaf, plus the use of a polyurethane adhesive formulated for cryogenic use, provide a satisfactory solution. Design details for the oeprational system remain to be optimized by further testing, however.

Our experimental approach is summarized in Table 4-1, and a schematic of the test arrangement is shown in Figure 4-1.

Table 4-1

SIRTF Optics Development Experimental Approach

Test Facility

- Modify existing thermal-vacuum test chamber to provide secondary shroud cooled to 10 to 20 K 34-in. diameter window aperture available.

Optical Test Configuration

- Finish mirror to smooth sphere of 175-in. radius, test at center of curvature with laser unequal path interferometer (LUPI). Concurrently test window by observing interference between front and rear surface reflections of a collimated beam.

Mirror Mount

- Tangent flexures designed to introduce less than 0.02-λ wavefront error on cooling of aluminum fixture and silica mirror

Mirror Cooling

- Copper braid, Invar buttons soldered to vacuum-evaporated chromium-nickel film on mirror backplate
- Liquid nitrogen, then helium-cryostat cooling of copper heat sink plate behind mirror.

FIGURE 4-1

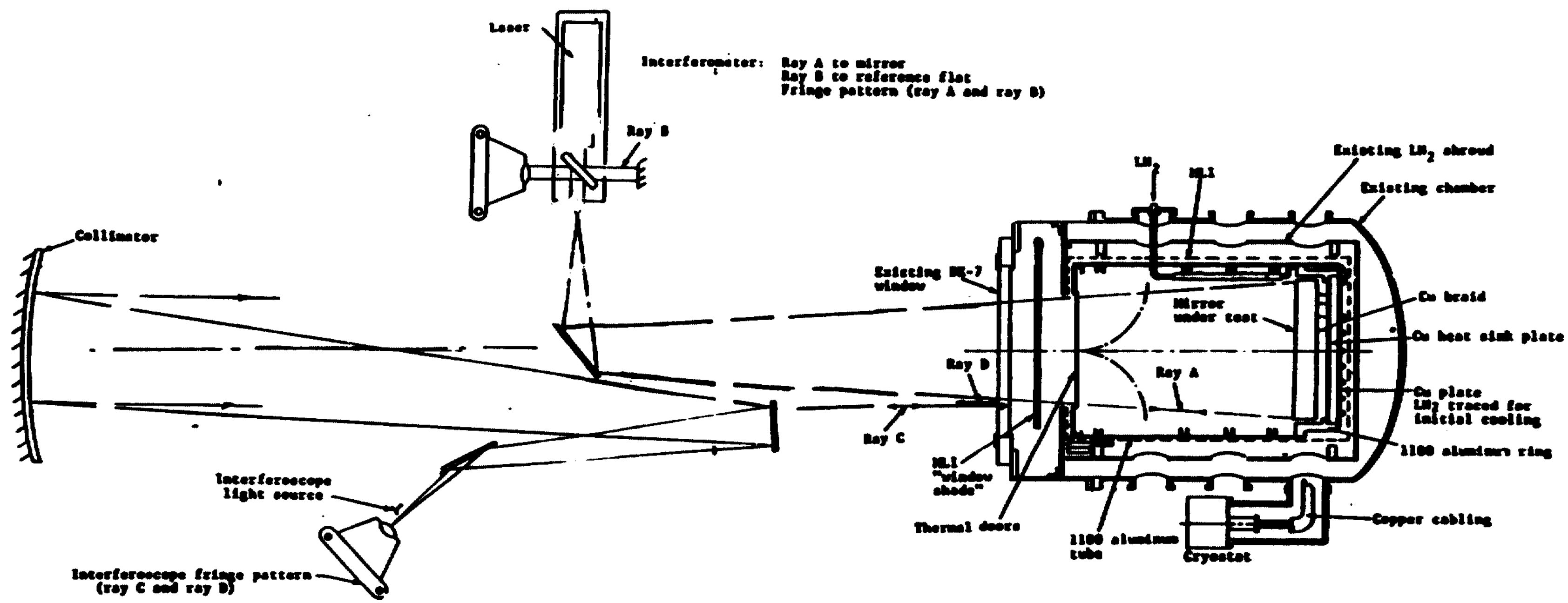

ORIGINAL PAGE IS OF POOR QUALITY

As the mechanical design developed, and estimates of the dimensions and mass of various parts could be made, a thermal mathematical model, including the variations with temperature of the conductivity and specific heat of the components, was assembled. System cooling was programmed as a two-stage operation. In the first stage, liquid nitrogen would be supplied to the outer shroud and the rear plate of the inner shroud. In the second stage, as the system approached 80 K, the rear plate would be purged while maintaining the liquid nitrogen supply to the outer shroud, and the cryostat would be put into operation. Component dimensions and masses were updated on completion of the manufacturing drawings, and the analyses rerun.

Results of the thermal analyses are included in Appendix A. The breadboard design verification tests undertaken to prove out the mount design, mirror thermal conductor design, other thermo-mechanical aspects and cryostat operation are described in Appendix B.

Details and comments on the temperature instrumentation are included in Appendix C.

5. RESULTS - FIRST COLD CYCLE

Liquid nitrogen first stage cooling was begun at 10:45AM on March 2, 1983. After 22 hours of operation, the inner shroud and mirror had reached near steady state temperatures of 89 and 93K, respectively, and cryostat cooling was started at 9:30AM on March 3, 1983.

Representative interferograms of the mirror plus window (one fringe = 1/2 wave surface displacement) and of the window alone (one fringe = 1/2 (n-1) n ≃ 1/6 wave equivalent mirror surface displacement) at room temperature* and with the mirror at approximately 13K are shown in Figure 5-1 (a-d). Temperatures indicated by the four silicon diodes on the mirror surfaces appear in Figure 5-2.

The most striking feature of these interferometric data, visible in Figure 5-1c and shown in more detail by the contour plots generated by digital data reduction, is the localized irregularity evident all around the outer area of the mirror. Figure 5-3, a surface contour map with 0.1 wave (633nm) contour intervals (heavy lines representing hills) illustrates these features. The hills correlate precisely with the hexagonal-celled structure of the mirror core. Further details of the reduced data are presented in Appendix D.

The silicon diode data show that the mirror temperature, at the rear surface and mid-point of the circumference, is rising quite rapidly - up to 0.6 kelvins per minute. Our curiosity eventually led us to examine the difference in two interferograms taken at 17:19:40 and 17:21:08, i.e. separated by one minute, 28 seconds in time on March 4, 1983. The contour plot resulting from this subtraction is shown in Figure 5-4. Here the contour interval is 0.25 waves (633nm); the data show that some of the hills rise, while others recede. The rms change in the surface is also striking, showing that the change occurring in little more than a minute approaches the magnitude we might have interpreted as the change incurred by the temperature

---

*As shown in Table D-1, Appendix D, the room temperature figure of the mirror, as mounted in the test chamber and under vacuum, was 0.10μm rms, compared to a desired value (para. 2.2.6 above) of 0.04μm rms. This "baseline error" is still readily subtracted, however.

excursion alone. (Although the magnitude and character of the room temperature to cold differencing were markedly different from our expectations.) Further discussion is deferred to Section 8 below.

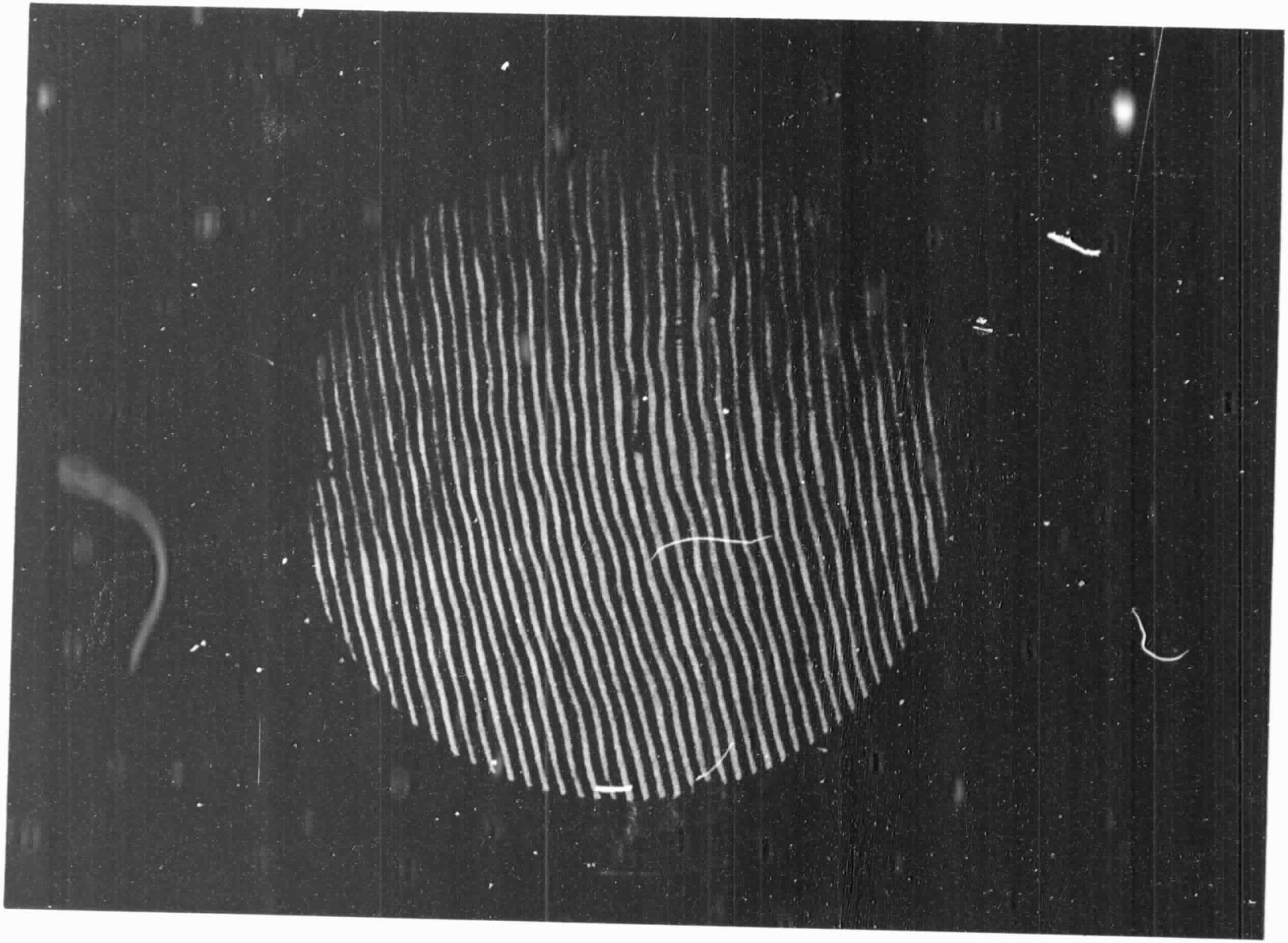

SIRTF MIRROR AND WINDOW INTERFEROGRAM
MIRROR AT ROOM TEMPERATURE
5-1a

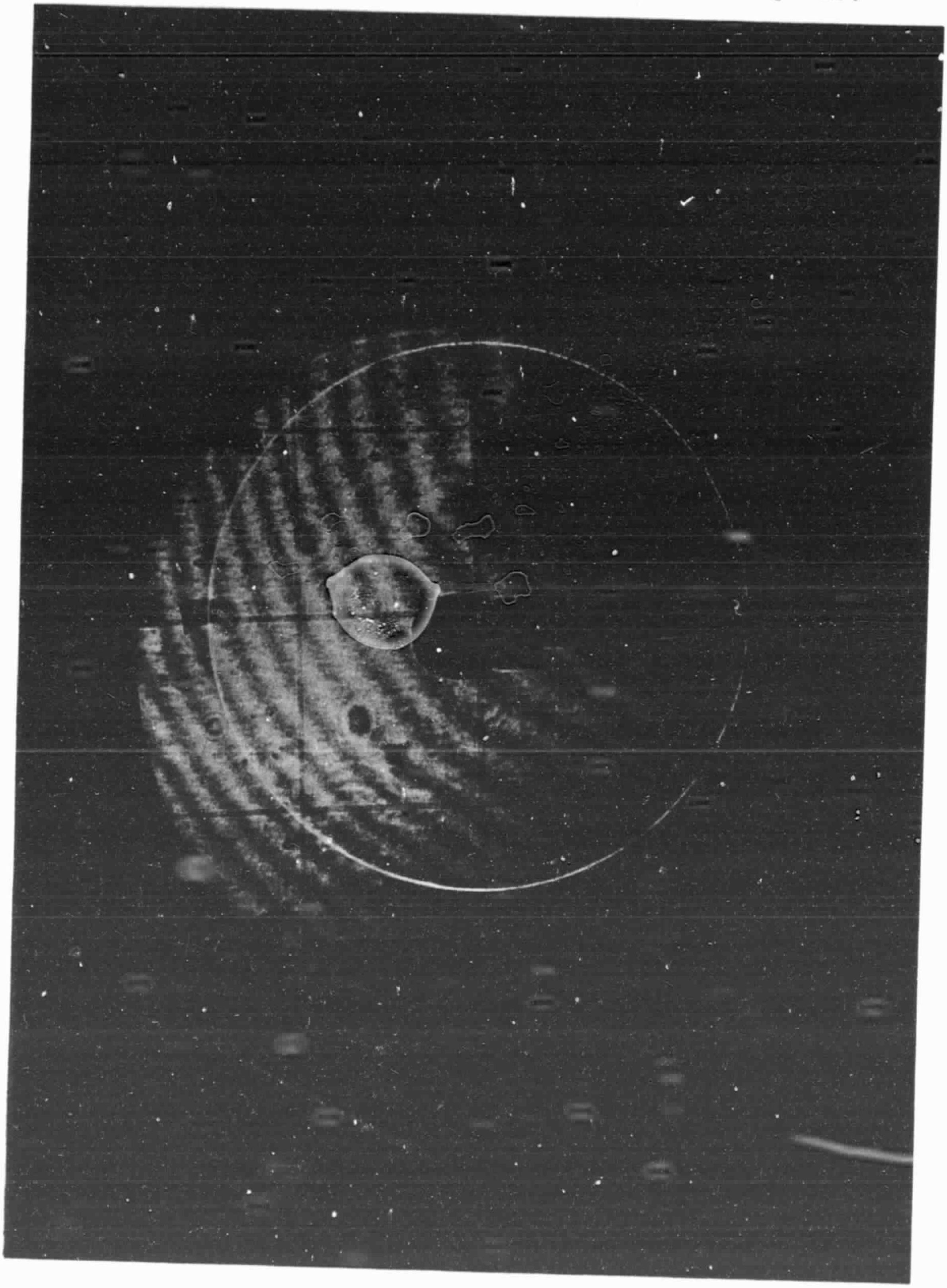

SIRTF WINDOW ONLY INTERFEROGRAM
AT ROOM TEMPERATURE
5-1b

ORIGINAL PAGE IS
OF POOR QUALITY

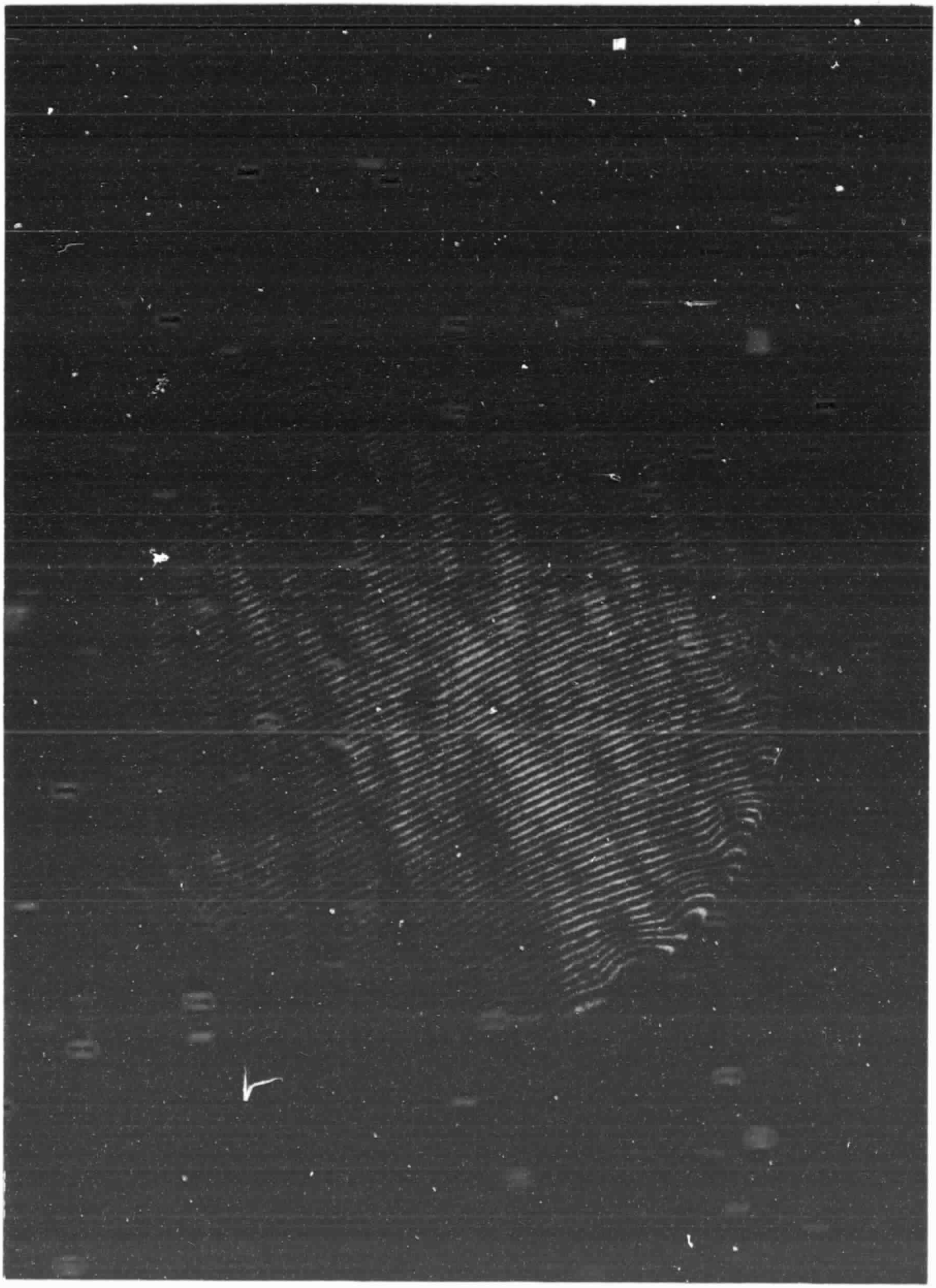

Digitized from original
as C83#0094
Taken at 17:20:43 on 3/4/83

SIRTF MIRROR AND WINDOW INTERFEROGRAM
AT LOW TEMPERATURE
5-1c

SIRTF WINDOW ONLY INTERFEROGRAM
MIRROR AT LOW TEMPERATURE
5-1d

BY:		TITLE: Mirror Temperatures	PAGE:
DEPT:	DATE:	15:30 - 16:30 hours, 3/4/83	PROJECT:

Curve	Diode	Location on Mirror
1	D4866	Rear, Center
2	D4948	Rear, 6 o'clock, near edge
3	D4781	Rear, 9 o'clock, near edge
4	D3880	Mid-side, 3 o'clock

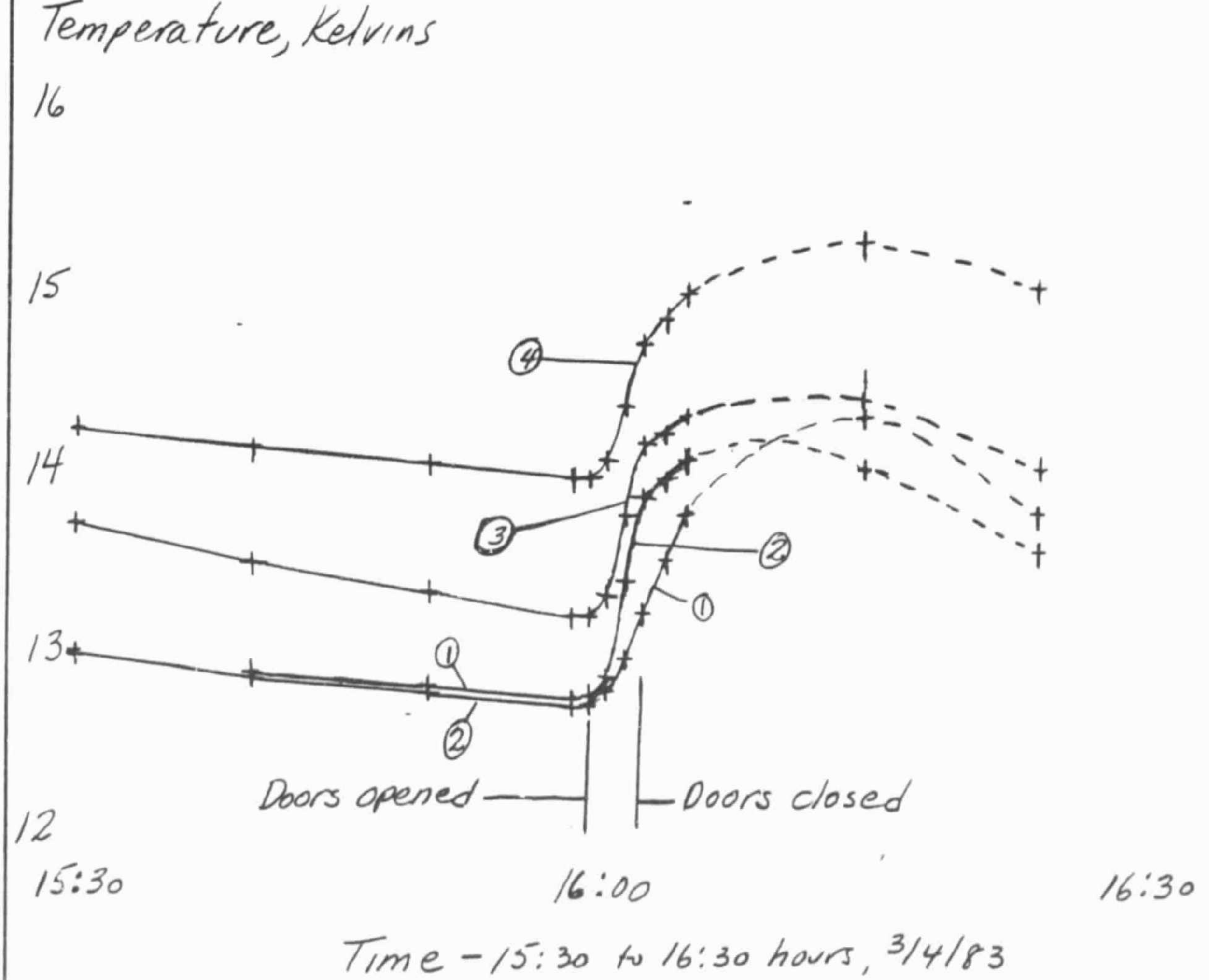

Figure 5-2a

BY:		TITLE: Mirror Temperatures 17:00 – 18:00 hrs 3/4/83	PAGE:
DEPT:	DATE:		PROJECT:

Curve	Diode	Location on Mirror
1	D4866	Rear, Center
2	D4948	Rear, 6 o'clock, near edge
3	D4781	Rear, 9 o'clock, near edge
4	D3880	Mid-side, 3 o'clock

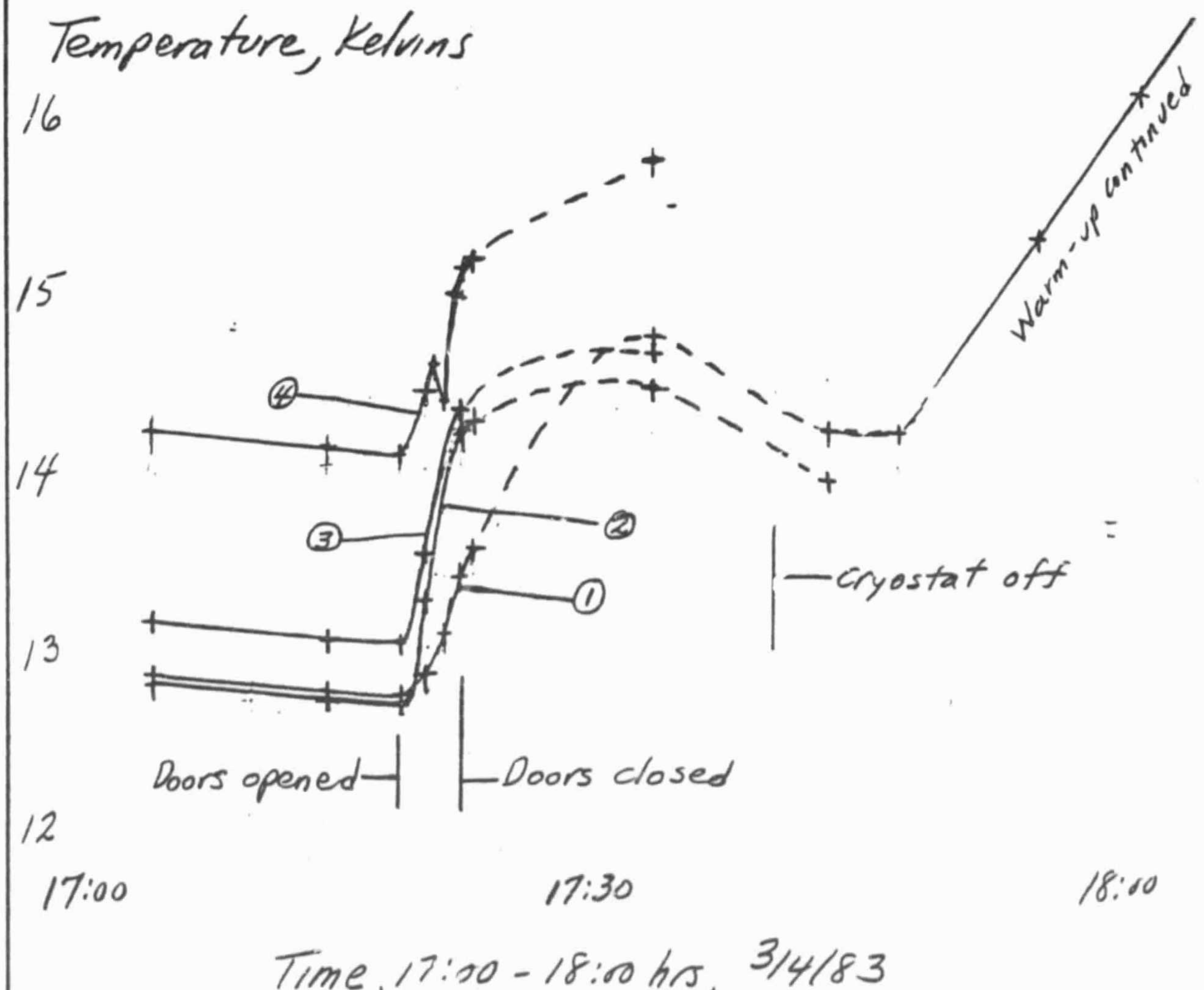

Figure 5-2b

E 103 REL 8/66 ENGINEERING ANALYSIS SHEET

0SFAD887 0PTICSG0 13*53*12 83.111 PLOT NUMBER 7

SUBTRACT SUBTRACT MINUS SUBTRACT

1

NONE (G) RMS 0.26 PKTPK 2.03 FRED SCALED

Figure 5-3

OSFRD056 OPTICSGO 09-59-22 83.130 PLOT NUMBER 4
SUBTRACT C83-0093 MINUS C83-0036
1
NONE (G) RMS 0.15 PKTPK 1.78 FRED SCALED

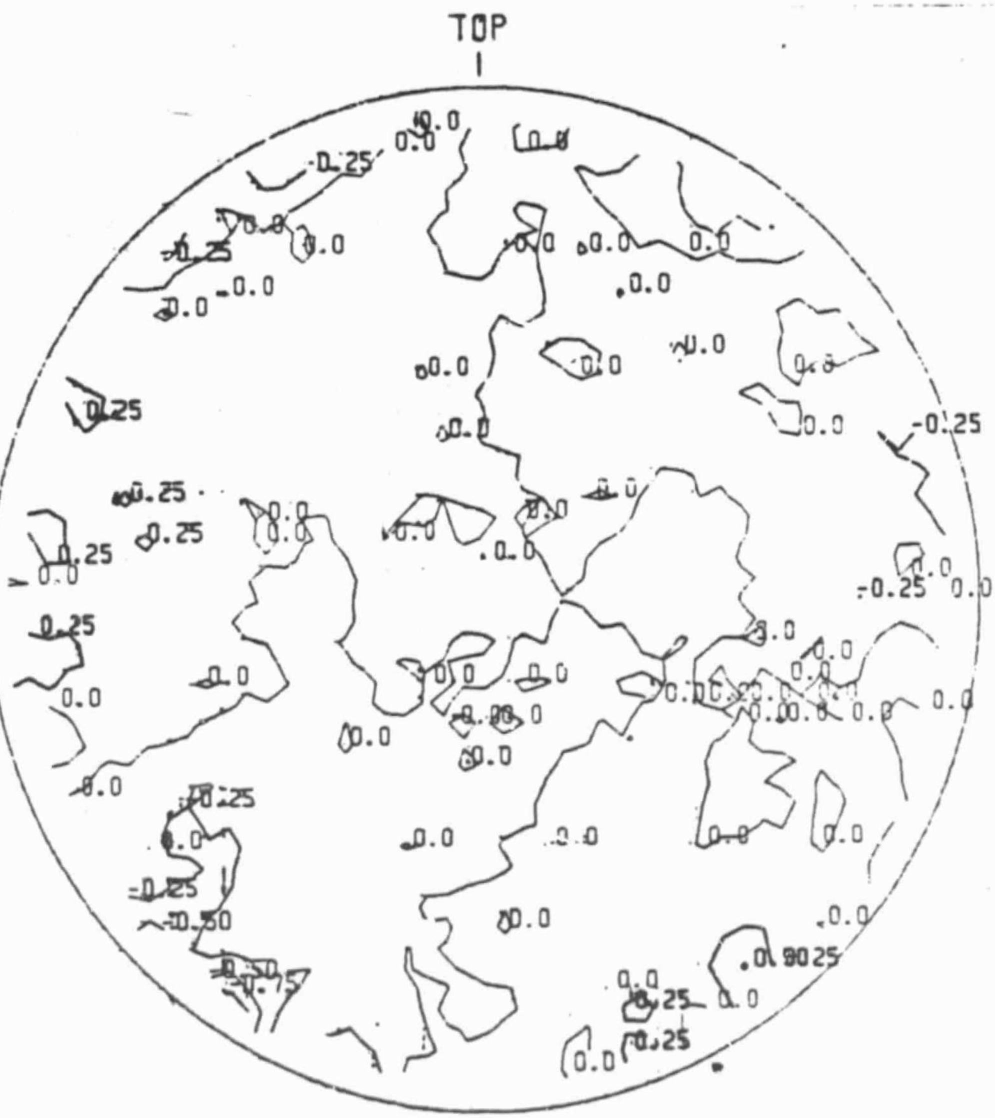

Figure 5-4

6. RESULTS - SECOND COLD CYCLE

Much of April was spent in reviewing the data collected in our first cold test sequence and discussing possible changes in test procedure which could improve our understanding of the thermal boundary conditions of the test. As a result, a contract amendment directing us to "make and analyze a real-time, video record or test interferometry" was issued.

The second cold test sequence was initiated on 16 May. Cooling proceeded at a somewhat slower rate than in the first test (approximately 8 hours longer to reach a mirror temperature of 15 K), and at 8:50AM on 19 May we first attempted to obtain a rapid sequence of Polaroid photographs of the interference pattern without adjusting the interferometer between exposures. Only the first of these proved useful, the returning wavefront from the mirror apparently moving out of register with the reference wavefront in the interferometer. This one photo, however, was substantially identical appearance to those of the first test sequence, and we then rearranged the test set-up for video recording of the interferometer pattern.

Some preliminary adjustments of the system were recorded at 10:39 and 11:15AM. After further allowance for thermal stabilization additional recording was done at 2:16 and 4:05PM. We attempted to preset the interferometer and video camera at focus through small holes in the thermal doors, but vibrations and drift during door operation required interferometer readjustments and prevented immediate recording of a fringe pattern as the doors were opened.

It was noted that the structure-correlated irregularities in the mirror surface, previously confined to the outer area, now appeared over the entire surface In the final two test sequences. We judged that some individual frames of the video record would be suitable for data reduction, in spite of significant vibration and wander of the fringe pattern, and passive warming of the system was started.

Post-test attempts to obtain single frame prints from the video tape have not yielded interferograms well-suited to digital data reduction, even though digital image processing was tried for removal of a quite noisy background from scatter and reflections in the video camera lens. Figure 6-1, a best focus, zero wedge fringe pattern captured during the 2:16PM test, provides the best available subjective picture of the mirror deflection (one fringe = 316nm surface deflection).

The thermal doors and "window shade" remained closed over night. At 9:01AM on May 20, a condensation pattern over part of the mirror was found, and an interferogram of the clear areas was recorded. At the time, the mirror temperature was about 160°K, and the thermal doors and "window shade" were left open to accelerate warming. Later (5:27PM) observation revealed condensation over the entire mirror, producing the scattering pattern shown in Figure 6-2. The scattering is more pronounced at the rib locations, indicating that these areas are colder than the face plate areas over the open cells of the mirror.

A final interferogram was made on 23 May, with the systems still under vacuum, but stabilized at room temperature (as indicated by thermocouple records).

Appendix E is a data summary for this second cold cycle. Fringe reduction data and contour plots for the interferograms of 8:56:05 on 5/19 and of 5/23/83 are included there, together with the temperature time histories of all data sequences of 5/19/83.

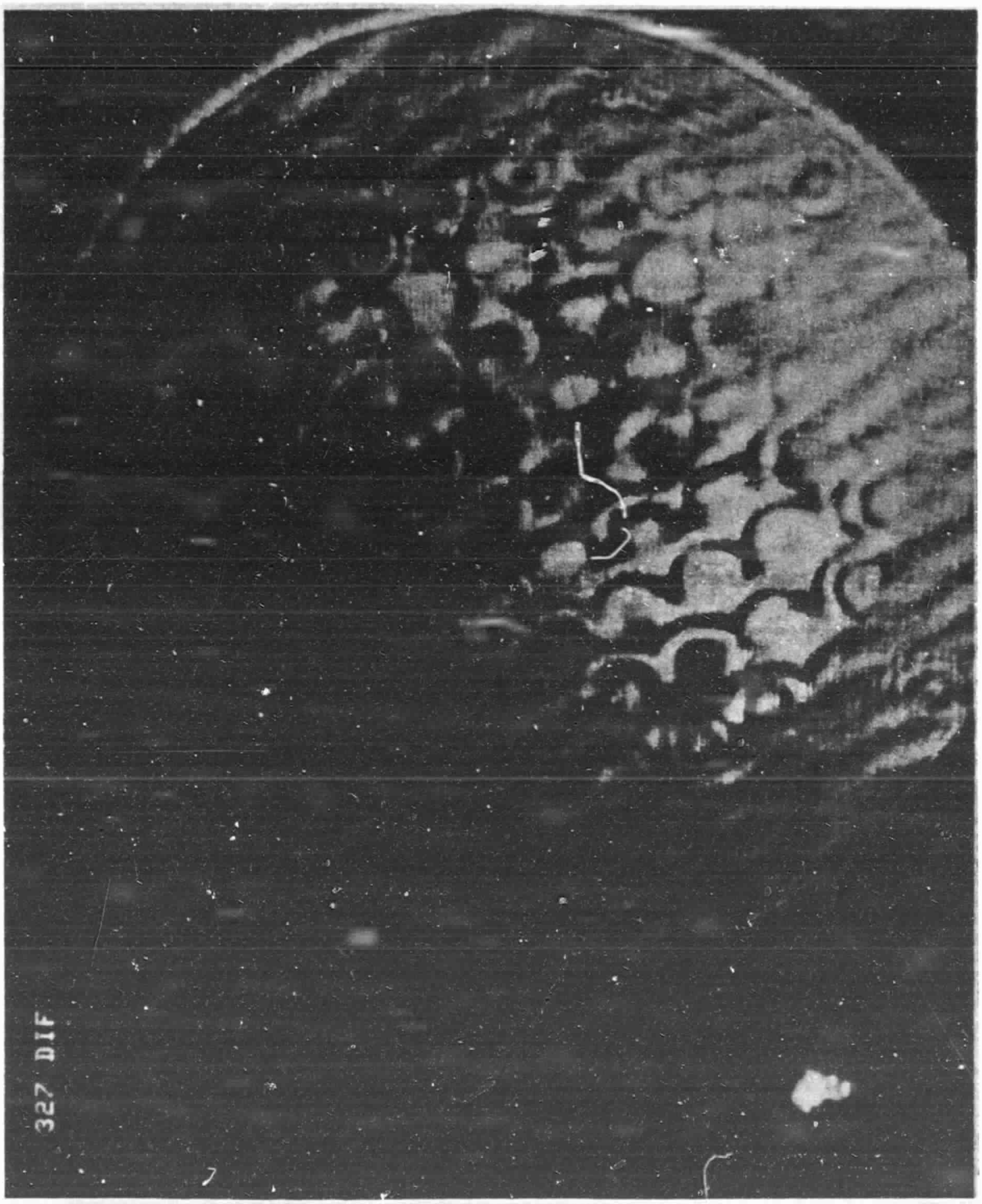

Figure 6-1

5/20/83 17:27 ~200K

T

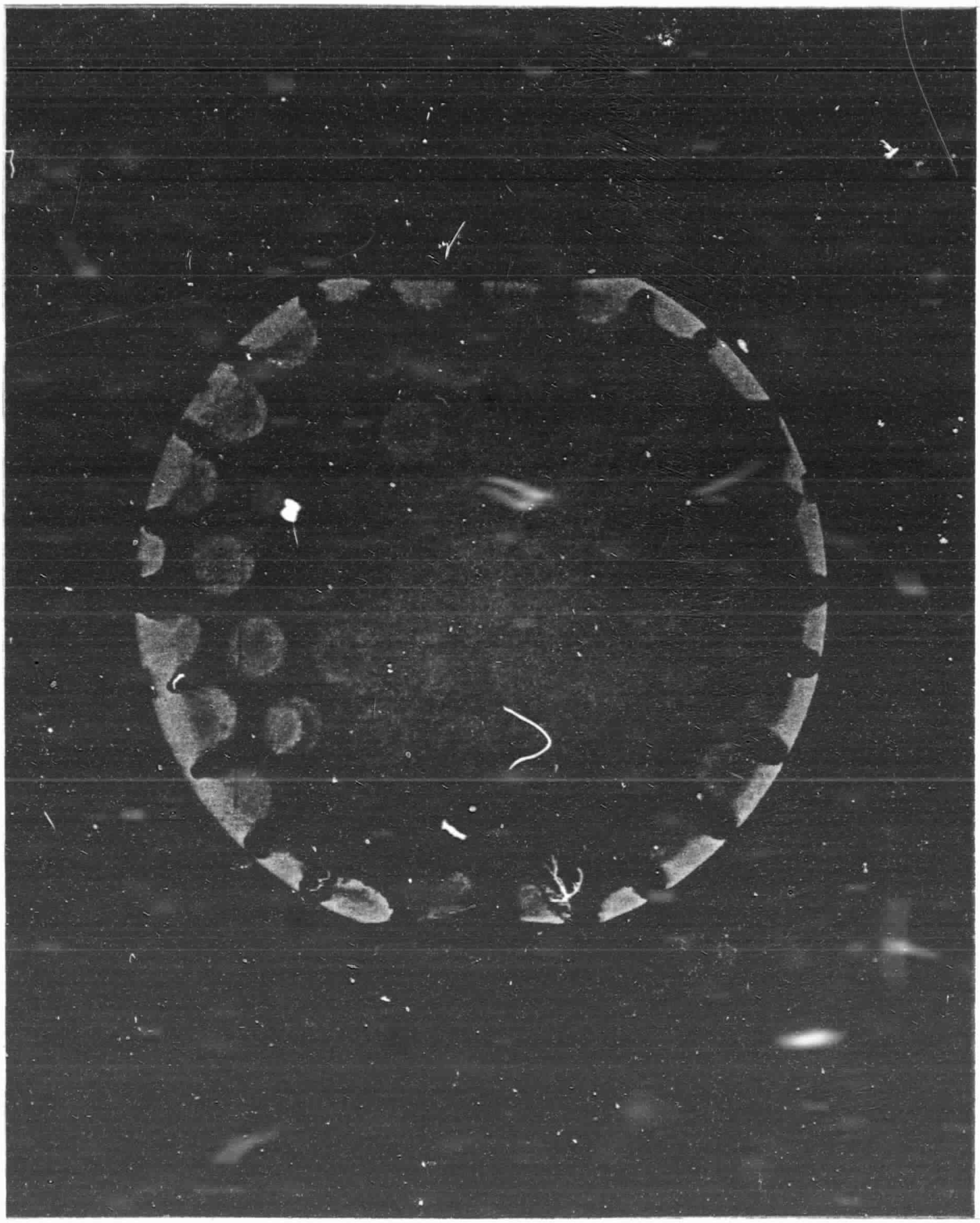

Figure 6-2

7. RESULTS - POST-TEST INSPECTION

We removed and inspected the mirror-flexure-aluminum ring assembly. A number of failures of the thermal conductor connections, indicating that the current design details of the soldering of Invar buttons to evaporated chrome-nickel-gold spots on the mirror may be marginal for the ultimate flight system. We had previously repaired some failures of these connections in initial assembly by direct ultrasonic soldering to the glass using an indium-tin eutectic. A total of 34 connections (out of 120) were thus repaired, 16 of these were noted as failed on disassembly, and an additional 4 came loose under light finger pressure. Of the 86 connections made to the evaporated spots, 2 were pulled off during disassembly, 12 were noted as having failed, and of the latter, 2 failures were fractures in the glass, not the joint. We have thus not demonstrated a complete solution to the thermal conductors needed for SIRTF, and further breadboard testing, possibly including combined low temperature and vibration testing, appears recommended.

Visual inspection of the flexure-mounts has shown no evidence of any damage or malfunction.

8. DISCUSSION AND CONCLUSIONS

As noted in Section 5 above, discussions following our design review had anticipated some perturbation of the mirror by the heat flux from the window, via the shroud and conductive paths to the rear surface of the mirror. On the basis of the more localized surface deflections seen on most of our interferograms, we believe that direct and multiply reflected radiative transfer from the window to the edge and rear surface of the mirror is also a significant factor. Some exploratory calculations show that this mechanism is plausible, but since our temperature data are limited, we have not been able to provide a detailed analysis of the mechanism causing the localized deflections.

The first observations supporting our speculations on the thermal boundary conditions at the mirror surface result from a differencing of successive interferograms taken while the thermal doors on the inner shroud remained open (FRED Summary Sheet Serial 058, Appendix B). These show that the mirror surface changes, over a period of one minute, were nearly equal to the differences between the first interferogram taken and the surface contour at room temperature. Temperatures indicated by the silicon diodes attached to the mirror, in the same time period, were changing at rates as high as 0.6 kelvins/minute. In spite of our provision of small holes in the doors to permit pre-focusing of the interferometer prior to door opening, we found that it required 60 to 90 seconds after full opening of the doors to adjust the interferometer and record the first fringe photograph. With some further consideration of the possible time scales of mirror response, this led us to the attempts, during our second test cycle, to obtain fringe data on video record as the doors were opened. Again, in spite of prefocusing, the minimum delay achieved between door opening and an even marginally readable fringe pattern was approximately 30 seconds.

To estimate the time required for at least localized thermal deflection equilibrium (not necessarily temperature equilibrium or even quasi-steady state) we examined the use of a thin slab, heated from one side. The temperature for this one dimensional case is given by*:

$$T = \frac{F_0 \ell}{k}\left\{\frac{Kt}{\ell^2} + \frac{3x^2-\ell^2}{6\ell^2} - \frac{2}{\pi^2}\sum_{n=1}^{\infty}\frac{(-1)^n}{n^2}\left(e^{-\frac{Kn^2\pi^2 t}{\ell^2}}\right)\cos\frac{n\pi x}{\ell}\right\}$$

T = temperature, K

F_0 = heat flux at $x=\ell$, W/m²

ℓ = slab thickness, m

k = thermal conductivity, W/m-K

K = thermal diffusivity, m²/sec

t = time

The curvature, γ, induced by this temperature distribution may be calculated from†:

$$\gamma = \frac{I_5 I_1 - I_4 I_2}{I_3 I_1 - I_2^2}$$

with

$$I_1 = \int_0^\ell dx = \ell \qquad I_4 = \int_0^\ell (\alpha T)\,dx$$

$$I_2 = \int_0^\ell x\,dx = \frac{\ell^2}{2} \qquad I_5 = \int_0^\ell (\alpha T)\,x\,dx$$

$$I_3 = \int_0^\ell x^2\,dx = \frac{\ell^3}{3}$$

Yielding

$$\gamma = \frac{\alpha F_0}{2k}\left\{1 - \frac{96}{\pi^4}\sum_{m=1}^{\infty}\left(\frac{1}{2m-1}\right)^4 e^{-\frac{(2m-1)^2 K\pi^2 t}{\ell^2}}\right\}$$

* Carslaw, H.S. and J.C. Jaeger, "Conduction of Heat in Solids", 2nd Edition, Clarendon Press, Article 3.8, para (i), Eq. 3. The solution is strictly valid, of course, only for constant k and K.

† APPLIED OPTICS, 5, 5, 701 (May 1966)

We see that as time increases, the temperature approaches a quasi-steady state, parabolic in x, and uniformly increasing in time, while the curvature approaches a constant value more rapidly because of the (2m-1) compared to (n) summation.

For a 5mm slab (the mirror faceplate thickness) of fused silica at 13 kelvins (κ=6.63 10^{-6}) and t=1 second, the summed terms yield the value 0.072. That is, 93% of the asymptotic value of the deflection of a 5mm section will occur within one second. For the full thickness of the mirror (0.1m), the (1-1/e) response time is only 2 1/2 minutes.

With respect to potential radiative transfer from the window (at 300K) to the unaluminized, and therefore quite black at 10µm. sides and rear surfaces of the mirror a number of paths are available. We had coated the inner window surface with a five-layer metal dielectric coating giving the following measured reflectances:

5µm	0.94
9µm	0.93
11µm	0.92
12.5µm	0.905
15µm	0.88
20µm	0.92
30µm	0.87
40µm	0.82

Integrating this times the black-body curve for 300 Kelvins yields an effective emissivity of 0.094. The total radiation from a 34-in. window aperture is then calculated to be 25 watts. About 1/4 of this will pass directly through the thermal door opening, and some smaller fraction goes directly to the approximately 2-in. annular opening between the edge of the mirror and the aluminum mounting ring. A number of multiple reflection paths also exist, however. Reflections between the outer MLI covering of the internal shroud and the window, and grazing incidence reflections from the inner surface of the shroud may contribute significantly. A rudimentary ray tracing shows that multiple reflections between the test mirror and window will also direct much additional energy just outside the mirror edge. With window and mirror reflectances of 0.9 and 0.98 respectively, those rays required to make 5 round trips still retain more than 1/2 their original energy density.

A direct observation of net heat fluxes to the mirror is provided by the silicon diode data, since the heat conduction equation may be written as:

$$\text{div } q = \frac{\partial(\rho CT)}{\partial t}$$

when q is the net heat flux to an elemental volume and ρCT is the enthalpy per unit volume. One should question whether the heat capacity of the diode itself or the material to which is is attached should be used here. We have tacitly assumed, that over our sampling times the diode temperature represents a substrate volume with a larger heat capacity than its own, and have thus used the ρC property of fused silica for the mirror diodes, and of aluminum for the one attached to the shroud tube. The results of these calculations of $(\rho CT)/\partial t$ are presented in Table 8-1. We were limited to four automatic recording channels for the diode data. In order to obtain some data on the shroud behavior, we switched one channel, after the first observation made on May 19, from the mirror rear center to the diode mounted on the inside of the shroud tube, near the mirror mount ring. Since the temperatures, and overall heat flux lévels varied, we also show the indicated heat flux values relative to the rear 6 o'clock mirror position in parentheses.

We make three observations from the relative flux data of Table 8-1:

a) the flux to the mirror center is lower than to the edge, consistent with less efficient paths for both radiative and conductive transfer from the window.

b) with one exception, the relative flux at 9 o'clock became smaller follwoing completion of the first observation sequence - this perhaps correlates with the subsequently discovered higher incidence of thermal conductor failures in the 9 o'clock area of the mirror.

c) a larger heat pulse occurred during the observation at 11:12AM on May 19 (intended for video checkout, rather than serious interferometry). The cause has not been established, but the higher relative flux values at the mirror edge and side, and lower value for the tube (compared to later runs) suggest

TABLE 8-1

ENTHALPY - TIME GRADIENTS

$\frac{\partial(\rho CT)}{\partial t}$ (J/m^3-s) At Silicon Diode Locations

(Relative values in parentheses)

Date	Time	Diodes on Mirror: Rear 4866 (Ctr)	Rear* 4948 (6 o'clock)	Rear 4781 (9 o'clock)	3880 (Side)	Diode on Tube 26306
3/4/83	16:24:10 to 16:25:17	211 (0.[illegible])	535 (1.00)	507 (0.95)	416 (0.78)	
3/4/83	17:44:03 to 17:45:09	292 (0.44)	661 (1.00)	511 (0.77)	496 (0.75)	
5/19/83	8:52:22 to 8:54:22	348 (0.33	1060 (1.00)	821 (0.77)	812 0.77	
5/19/83	11:12:09 to 11:13:09		1854 (1.00)	1709 (0.92)	2279 (1.23)	3870 (2.09)
5/19/83	14:11:49 to 14:12:49		725 (1.00)	568 (0.78)	502 (0.69)	2740 (3.78)
5/19/83	16:01:38 to 16:03:38		988 (1.00)	788 (0.80)	775 (0.78)	3532 (3.84)

that the radiation transfer was increased in this case.

As a final first order quantitative estimate, if we assume that a value of $\partial(\rho CT)/\partial t$ of 600 J/m^3-s results from flux to one side only of a 5mm slab, and that the quasi-steady parabolic gradient has been established, then we have

$$\frac{\partial(\rho CT)}{\partial t} = \frac{\partial}{\partial t}(\rho C)\left(\frac{F_0 \ell}{k} \times \frac{Kt}{\ell^2}\right) = \frac{F_0}{\ell}$$

yielding $F_0 = 3\ W/m^2$

The curvature induced is:

$$\gamma = \frac{\alpha F_0}{2k} = \frac{-0.5(10^{-6})(3)}{2(0.12)} = 6.25(10^{-6})\ m^{-1}$$

and over the 3.25 inch (82.6mm) diameter of the cells of the mirror core, a total deflection of 5.3 (10^{-9})m (0.008 waves at 633nm) would be produced. This is roughly two orders of magnitude below the observed intracellular deflections. Part of the discrepancy may lie in the diode locations, which are closer to the edge ring than to the center of the cells. We do not feel, however, that we have developed a full understanding of the mechanisms causing the observed deflections. We retain, however, a strong conviction that they are not caused by inhomogeneities of material properties, poor fusion, or other mirror blank imperfections.

Although our test results have revealed some short comings in precise control of thermal flux boundary conditions, and a somewhat unexpected speed of response of the thermal bending of the mirror, we have shown that our conductor and mount designs are at least marginally acceptable for operational use. The results may, in fact, be preferable to complete, unequivocal success, since we would then have no information about the possible level of over-design present.

9. RECOMMENDATIONS

Two items of engineering development suggest themselves immediately. The conductor failures recommend a study of design modifications, such as the use of the flexible polyurethane (used in the mounts) as a bonding agent - a metallic bond is not really necessary. Breadboard testing of such modifications should include concurrent exposure to low temperature and vibration environments. Secondly, our results cannot separate mirror deflections caused directly by the thermal environment from those which may be transmitted through the mounting flexures. Thus a series of tests of the mirror deflection response to controlled deflections of the mount ring would provide a needed better knowledge of mounting effects.

APPENDIX A

TEST SYSTEM THERMAL ANALYSES

The system thermal model is shown in Figure A-1, and the thermal analysis results for the two-stage cooldown are shown in Figure A-2. In the second stage (cryostat cooled) the shroud tube and thermal door temperatures are quite close to that of the primary mirror. We estimated that the total time required for cooling from 293 to 20K would be 24 hours.* The elements of a steady-state cryostat load at 20K of 1.532 W are shown in Table A-1. The design capacity of the cryostat at 20 K is 9 to 12 W; thus we believe overall thermal design was conservative, and the 20 K goal should be achievable.

*Actual test operations required 50 to 60 hours to bring the mirror temperature below 20 Kelvins.

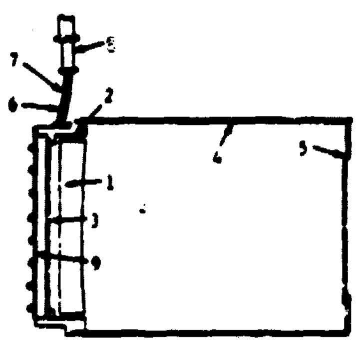

Node	Description	Material
1	Primary mirror	Fused silica
2	Mirror bezel	1100 aluminum
3	Mirror conductor plate	Copper
4	Tube	1100 aluminum
5	Aperture end, doors	1100 aluminum
6,7	Braid	Copper
8	Cryostat, CTI 1020	
9	LN_2 plate	Copper

Figure A-1

Test Configuration System Thermal Model

ORIGINAL PAGE IS
OF POOR QUALITY

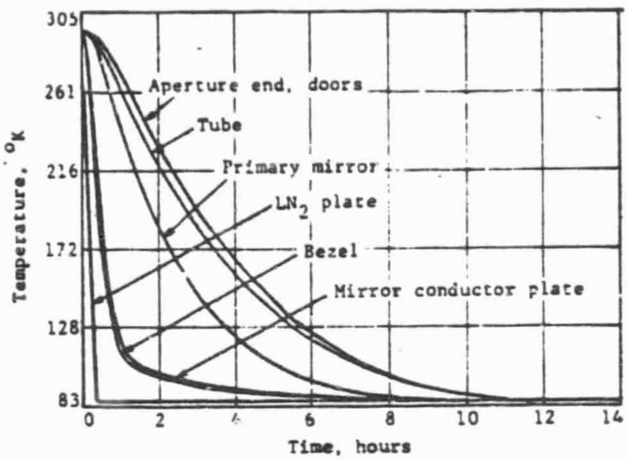

First stage cooling

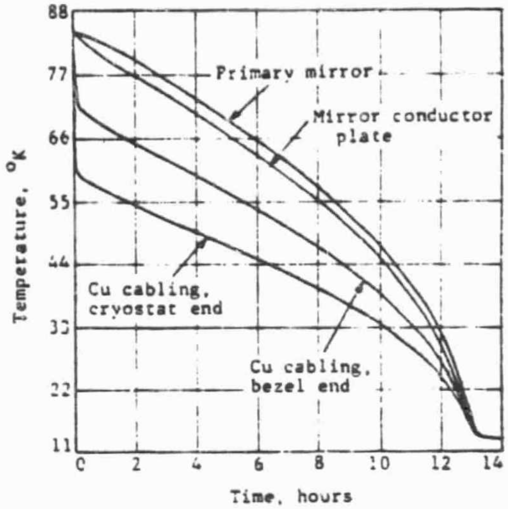

Second stage cooling

Figure A-2

Thermal Analysis Results for Two-stage Cooldown

Source	Heat Transfer Mode	Heat Load, watts
MLI	Radiation	0.161
Tripod supports (9)	Conduction	0.418
LN_2 tubing (2)	Conduction	0.489
Aperture (closed)		
Shutter surface	Radiation	0.219
Shutter edges/gap	Radiation	0.023
Shutter holes (four 2-in. diameter)	Radiation	0.018
Shutter motor drive shaft	Conduction	0.096
Thermal instrumentation	Conduction	0.108
Total heat load at 20°K, watts Steady-state condition		1.532

Table A-1

Steady-State Heat Load on Cryostat at TLSI Temperature

During the early design review conducted at the NASA Ames Research Center, a question was raised whether the estimates of the focal shift of the fused silica mirror upon opening of the thermal door had adequately accounted for all of the potential heat flux paths. The radiative flux, from the chamber window to the cryostat-cooled shroud, which is then conducted to the rear of the mirror, was identified as a perturbation that had not been sufficiently analyzed. Actually, two major changes in the thermal boundary conditions necessarily occur when optical observation is begun--the thermal door is opened, exposing the approximately 300K window to the mirror and the interior of the shroud and, at the same time, the cryostat is shut down to eliminate its vibration input.

These boundary conditions were applied to the system thermal model, and all of the parasitic heat leaks we have identified were also included. For an initial uniform temperature of 25K, the temperature histories for nodes 1 to 4--mirror, bezel, copper plate for mirror conductive attachments, and shrcud--are shown in Figure A-3. The results of this run also indicate that the heat flux through the flexures to the mirror is (at a quasi-steady state) 0.032 W, compared to a flux of 1.4 W via the conductive connection to the rear face of the mirror.

Figure A-3

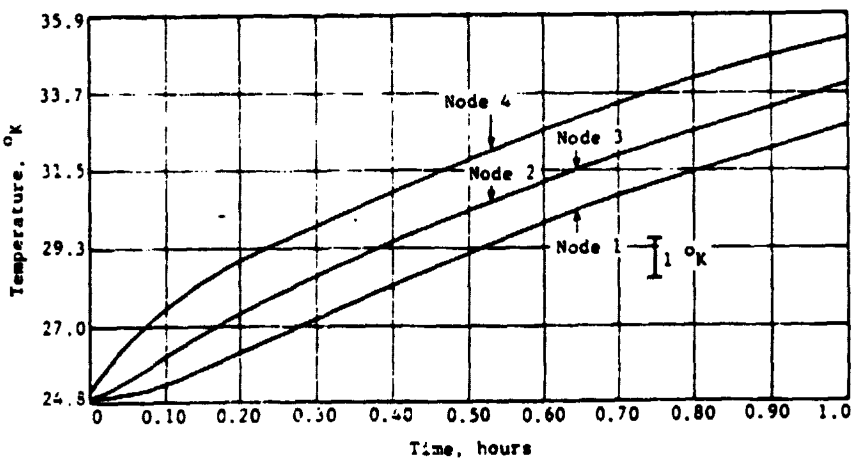

Temperature Histores - Thermal Doors Open, Cryostat Off

This latter conductive flux, and the previously modeled direct radiation from the window to the mirror front surface, were then applied as time-varying boundary conditions to the more detailed mirror model. The results, presented in Figure A-4, indicate that an axial temperature gradient develops at a moderate rate but does not reach a steady gradient in the analysis time of 1 hour.

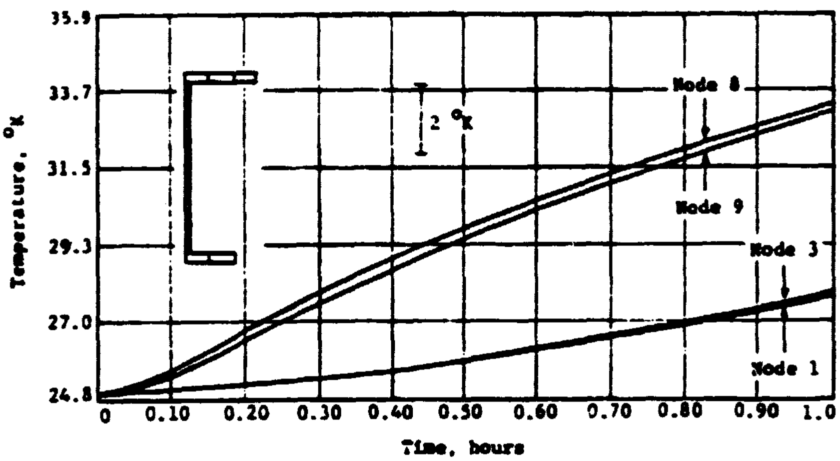

Figure A-4

SIRTF Primary Mirror Thermal Model

The principal result of this axial gradient is a change in the overall curvature of the mirror. The change in the number of optical power fringes observed may be estimated as:

$$\Delta N = \frac{\varepsilon(\text{node } 1) - \varepsilon(\text{node } 8)}{(\lambda/2)} \frac{d^2}{8\ h}$$

In the 0 to 40°K range, the thermal strain of fused silica is closely represented by:

$$\varepsilon(T) - (46 - 0.01125T^2)\ 10^{-6}$$

combining these relations, we obtain for our 26-in. aperture, 3.5-in.-thick test mirror

$$\Delta N = 0.0192\ (T_8{}^2 - T_1{}^2)$$

The results (Figure A-5) show that the optical power change induced by the changed boundary conditions is sufficiently small and slowly developing that it can be readily removed as part of the data reduction process or by some slight refocussing of the interferometer. Perturbations from lateral gradients, which would require considerable effort to model adequately, were expected to be much smaller than the few fringes per hour of this principal perturbation.

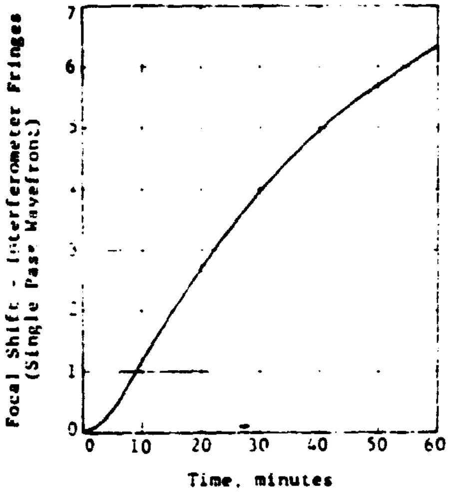

Figure A-5

Interferometer fringe shift with thermal shutter open (initial temperature 25K)

APPENDIX B

COMPONENT VERIFICATION TESTS

B.1 Flexure Mounting

An important goal is a demonstration that the mount design is suitable for use with a fused silica mirror in an aluminum telescope structure. Our mount design included a flexure pivot and flexure leaf copied from Teal Ruby but sized, in aluminum, to accommodate the differential expansion, radially in the pivot, between aluminum and fused silica for the 293 to 20°K range without subjecting either material to excessive stress. To check the design, we included testing, by liquid nitrogen immersion, of a breadboard flexure assembly prior to final assembly of the mirror.

A first breadboard of a fused silica boss, aluminum flexure pivot, and aluminum flexure leaf was assembled with PR-1660 polyurethane adhesive.* The fused silica surfaces were left as generated by a 150-grit diamond wheel, since our design was intended to keep stresses low. After five cycles of immersion in liquid nitrogen, a pair of localized fractures on the silica were found under each of the four feet of the flexure pivot, at the pivot-silica bond. This result is shown in Figure B-1--the fractures are ascribed to the lateral shrinkage of the aluminum. Strong, noncompliant bonding of a high-expansion material directly to fused silica is obviously not recommended.

In the belief that an Invar pivot would solve the problem at the glass interface and still be compatible with an aluminum flexure leaf, we fabricated and assembled this combination using the same adhesive. On the fourth immersion cycle an audible fracture occurred following about 8 min. of slow immersion, about 20 sec after immersion was complete. In addition to a major fracture believed caused by radial compression and stress concentration where the boss joins the parent material, we found one small fracture having a morphology similar to that caused by the aluminum pivot.

Additional fused silica test items were made up, and the metal parts disassembled by an immersion in warm orthodichlorobenzene.

---

*Products Research and Chemical Corporation

27722

Figure B1 - Aluminum Pivot/
Aluminum Leaf

The following changes in the assembly procedure were then made:

1. The fused silica parts were etched in hydrofluoric acid to remove approximately 0.005 in. from the as-generated surfaces and

2. A polyurethane adhesive specifically formulated for cryogenic use was substituted (PR-1578--its elongation at tensile failure is 7 to 8% at 77°K).

The etching not only strengthened the glass, but also provided a larger gap to be filled by the more compliant adhesive. Both the aluminum and Invar pivot assemblies were made up slightly decentered from the silica boss, so that adhesive layers of 0.003, 0.006 and 0.009 in. were present in both assemblies.

These assemblies were again tested by cycling into liquid nitrogen, this time being held in the cold vapor for 1 hour before immersion (although we had no evidence that thermal shock had been a significant factor in the previous failures). The aluminum assembly again failed, on the first immersion cycle and with similar morphology, as before. It does appear, however, that the severity of the fractures is less for the thicker adhesive layers.

The Invar pivot assembly was further tested by immersion in liquid helium, and no evidence of fracture or debonding was observed.

B.2 Conductive Connectors

The copper braid conductive connections were proposed as an Invar button and braided copper wire soldered to vacuum-coated chromium-nickel-gold spots on the rear surface of the mirror. To verify their strength and low-temperature survivability, we made up a number of test specimens consisting of 1-3/16 in.-diameter, 1/4-in.-thick discs of fused silica obtained from the residual core-drilled pieces of the mirror we plan to test. To each we applied a 1/8-in.-diameter spot consisting of successive layers of chromium, nickel, and gold by vacuum evaporation. An Invar (and in some cases, copper) button, previously soldered to the end of a length of braided copper wire, was soldered to the coated spot, as shown in Figure B-2.

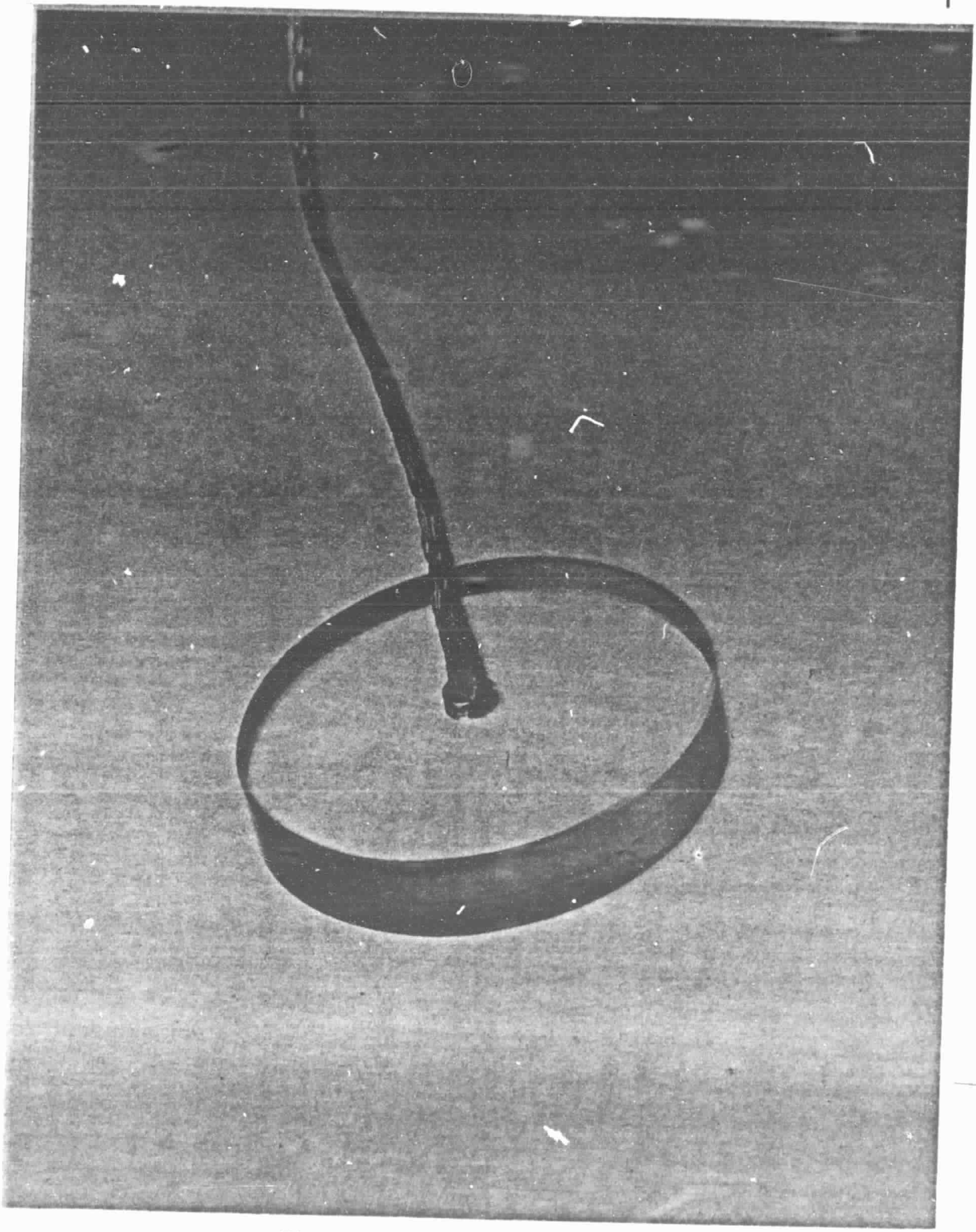

Figure B2 - Thermal Conductor
Test Specimen

After some preliminary trials, nine specimens were prepared using different solders for the button-to-glass joint as shown in Table B-1. All were dead-load tested with 1 to 1.6kg loads, and cycled five times into liquid nitrogen. One failure occurred in this thermal cycling. Specimen nos. 2, 3, 4, 5, and 9 were then tested in tension using an Instron Universal Testing Maching with results as summarized in Table B-2.

Table B-1

Breadboard Conductor Specimens

Specimen No.	Coating Batch	Button	Braid/Button	Button/Glass	Dead Load Test, kg	Remarks
1	Trial	Invar	60 Sn/40 Pb	60 Sn/40 Pb	1.06	Separated in fourth LN_2 Cycle
2	Trial	Invar	60 Sn/40 Pb	52 In/48 Sn (wire)	1.06	Does not seem to wet as well as 60/40
3	No. 1	Invar	60/40	60/40	1.215	
4	No. 1	Invar	60/40	100 In (cream)	1.663	
5	No. 1	Invar	60/40	80 In/15 Pb/ 5 Ag (cream)	1.663	
6	No. 2	Copper	60/40	60/40	1.663	Button off center of coating. Broke, pulled out glass.
7	No. 1	Invar	60/40	52 In/48 Sn	See remarks	Tried tinning glass directly. Pulled off by hand. Reattached to coated spot, held 1.663 kg.
8	No. 1	Copper	60/40	60/40	1.663	
9	No. 1	Copper	60/40	100 In (cream)	1.663	
						All except six cycled 5X in LN_2. No. 1 failed on fourth cycle. All others survived without apparent damage and nos. 2, 3, 4, 5 and 9 were tested to destruction by tension on braid.

ORIGINAL PAGE IS OF POOR QUALITY

ORIGINAL PAGE IS
OF POOR QUALITY

Table B-2

Instron Test Results

Specimen No.	Test No.	Tension Load Reached, lbs	Failure Mode
2	1	8.9	Break at bond area
	1	20.0	No break
	2	27.0	Break in braid at grips
3	3	31.5	No break
	4	31.3	Break in braid at grips
	5	31.4	Break within glass
4	1	20.8	Break in braid below button
5	1	20.4	Break at bond area
9	1	23.[illegible]	Break at bond area

The higher strength of the 60/40 solder joints, the fact that even copper buttons so soldered survived immersion in liquid nitrogen, and the somewhat better wettability as compared to the indium solders suggest that this most common electronic grade solder may be used throughout conductive connections of this size. We speculate, however, that connection of larger elements of high-expansion materials might fail, since the 60/40 solder becomes embrittled at about 180°K.

B-3 Cryostat-joint Conductance Test

An off-line test of a mockup of the cryostat conductor connections was added to the contractually required tasks early in 1982. Three purposes were served by this test:

1. Verification that the joint design would give good thermal conductance down to 10°K
2. Verification of cooling cpaacity of the cryostat we planned to use.

3. Development of experience with silicon diode temperature sensors and their comparison with thermocouple and platinum resistance thermometer measurement.

The assembled mockup is shown in Figure B-3.

This assembly was enclosed in an aluminum cover, wrapped with several layers of superinsulation, and mounted via the cryostat external flange to one of Itek's larger vacuum coating chambers. Conductively coated mylar heaters provided an adjustable thermal load. All test joints were made up (as designed) with 0.005-in.-thick pure tin washers in the joint and Belleville washers under the nuts. The assembly was joined to the cryostat through an indium washer.

Three of the four test joints exhibited conductances of 1 W/cm -K or more at 10 to 30 K. Data for the fourth joint appeared anomalous as the test was run. On disassembly, we found that a steel washer had been omitted, making the contact area of this joint much smaller than planned.

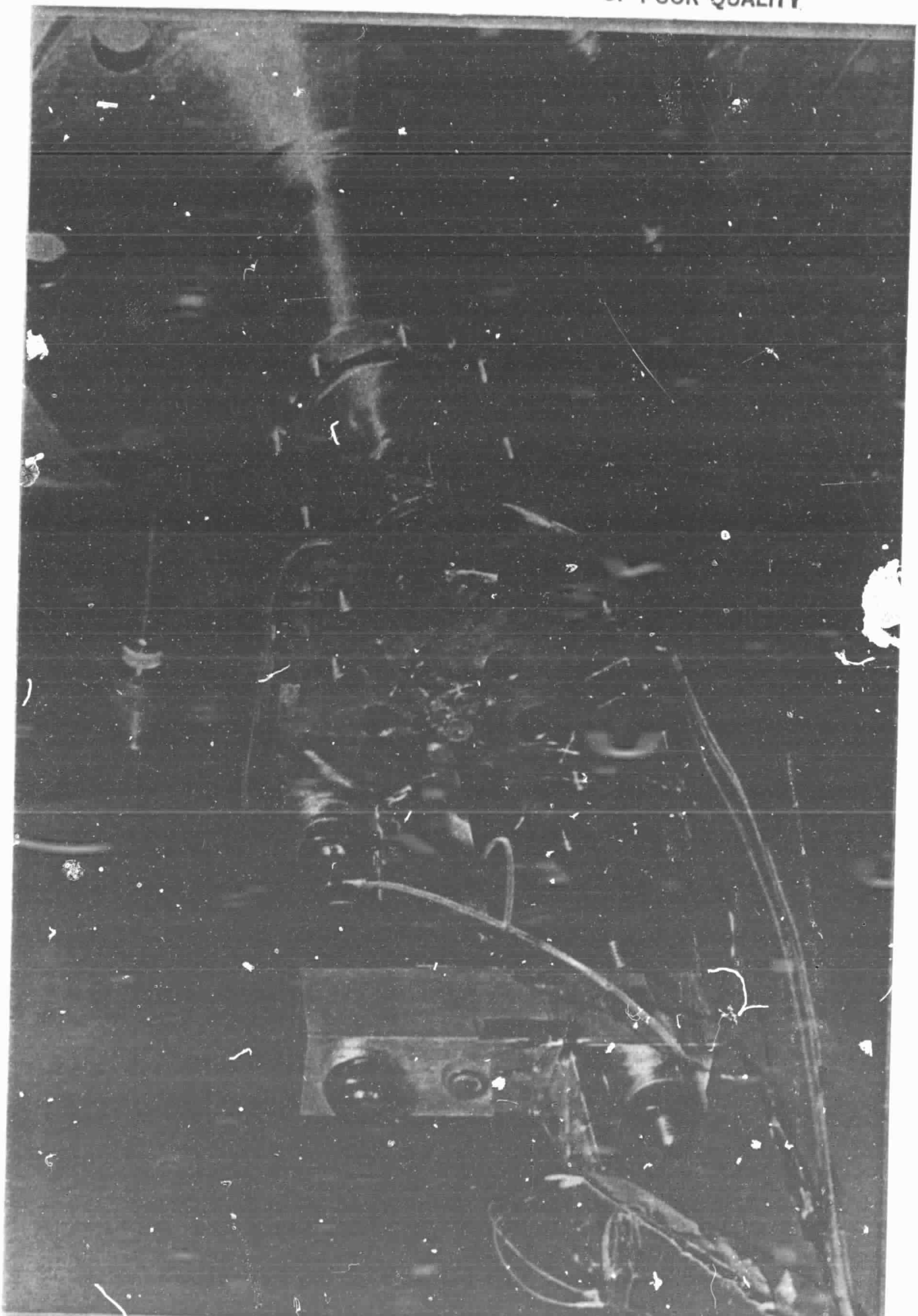

27889-21

Figure B3

APPENDIX C

TEMPERATURE INSTRUMENTATION

The temperature sensors used consisted of nine silicon diodes (Lake Shore Cryogenics Model D500-Cu) and 37 Type E chromel-alumel thermocouples. Of the diodes, five were manufacturer calibrated and supplied by NASA Ames, together with two five channel constant current power supplies. An additional calibrated diode was not used because it gave erratic readings in our off-line cryostat tests. The remaining four diodes were uncalibrated diodes referenced to the calibration of diode D 3880 using the data from the off-line cryostat-joint conductance test.

The thermocouples were attached to a data-logger with direct readout in Celsius or Fahrenheit degrees, with all channels recorded automatically. The diodes were connected to a 4-channel printing voltmeter reading to 0.1 millivolt. Manual switching was used to record those diode signals not being read automatically. During the first test runs the four diodes on the mirror were read automatically. After the first test of the second sequence, the diode attached to the shroud tube was read in place of that on the center of the mirror rear surface. Diode and thermocouple locations are listed in Table C-1.

The thermocouples develop substantial systematic errors at temperatures below 50 Kelvins because of the low e.m.f. being generated. They were thus used primarily to track the first stage (LN_2) cool down and will not be reported in detail here.

Plots of the temperature-time behavior at selected points, and a discussion of their significance are included in the body of this report.

TABLE C-1

SIRTF Thermal Sensors

Silicon Diodes #	Sensor #	Location:
1	D4866	Mirror, Center, Backplate
2	D4948	, Bottom, Backplate, 6 o'clock
3	D4781	, Left, Backplate, 9 o'clock
4	D3880	, Periphery, Right, 3 o'clock
5	D4780	Bezel, Inside, Right, 3 o'clock
6	Z6312	Cu Conductor Plate, Edge, Right, 3 o'clock
7	Z6306	Tube, Inside, Rear, Right, 3 o'clock
8	Z6307	Braid, Block at Bezel
9	Z6311	Cryostat, Cold Stage Flange

Thermocouples (3 Mil, Type E)

32	Adjacent to Diode #1
31	#2
33	#3
36	#4
34	Window, Inside Surface, at ℄
35	, 9½" from ℄ at 6 o'clock

Thermocouples (30 Gauge, Type E)

1	Cu Conductor Plate, Center
2	, Right
3	, Left
4	LN_2 Plate, Center
5	, Right
6	, Left
7	Tube, Inside, Centered, Right
8	, Left
9	, Forward, Right

TABLE C-1 (cont'd)

<u>Thermocouples (30 Gauge, Type E)</u>

10	Door Annulus, Inside, Right
11	Door, Right
12	80K Shroud, Centered, Right
13	, Top
14	, Rear, Centered
15	, At FWD. Left Support
16	80K Door Shroud, Top
17	Copper Plate
18	Braid Flange, at Cryocooler End
19	, at Bezel End
20	80K Door Shroud, Bottom
21	Shade, Top
22	, At Optical Centerline
23	Window Bezel, Bottom
24	, Top
25	Chamber, at Left FWD 80K Shroud Support
26	80K Shroud Rail, Center
27	80K Shroud, Centered, Left
28	Window, Inside Surface, 10½" from ℄ at 12 o'clock
29	, at 3 o'clock
30	, at 6 o'clock
37	Window, Outside Surface, Opposite #29

APPENDIX D

INTERFEROMETRIC DATA REDUCTION - FIRST COLD CYCLE

The interferograms were reduced to surface deflection components (cylinder, coma, tricorn, r^4) and contour maps using Itek Optical Systems FRED (Fringe REDuction) Program. Subtractions were performed point-by-point after tilt and nearest sphere (area weighted rms minimum) components were removed and the data interpolated to a 50x50 grid overlaid on the circular aperture.

Examination of these data can be tedious, and we have selected those items which illustrate all of the important changes observed with a minimum of repetition. We do not want to present a tutorial on examination of all of the data components, and believe that most readers will be able to form their own judgements on the significance of the data by examining the contour plots presented. We have also summarized the values of and changes in the "low frequency" components in Table A-1 with the caution that the significance attributed to differences (in particular) should not be pushed much beyond 0.1 wave - in most cases, one significant digit. Also, note that in all cases, the indicated changes in focus are not significant since it was usually necessary to reposition or refocus the interferometer for each photograph.

ORIGINAL PAGE IS
OF POOR QUALITY

Table D-1

SUMMARY OF VALUES OF DIFFERENCES OF "LOW-FREQUENCY" MIRROR SURFACE CONTOUR COMPONENTS

Contour Components Peak-to-Peak Waves (633 nm)

Figure No.	Mirror Temp.	Time/Date	Cylinder Amount	Cylinder Angle	Coma Amount	Coma Angle	Tricorn Amount	Tricorn Angle	r^4	R.M.S. After focus fit only
D-1	Room	0900 3-2-83	0.534	83°	0.124	216°	0.143	44°	-1.130	0.159
D-2	~13 K	1600 3-4-83	0.091	39°	0.875	139°	0.215	88°	-0.615	0.206
(D-3-3) = (D-2)-(D-1)			0.540	178°	0.855	131°	0.328	94°	+0.515	0.259
D-4	~13 K	17:19:40 3-4-83	0.974	49°	0.798	126°	0.273	90°	+0.114	0.277
D-5 = (D-4)-(D-1)			0.927	33°	0.806	117°	0.391	95°	+1.243	0.306
D-6	~ 13K	1600 3-4-83 0.75 dia aperture	0.128	34°	0.580	139°	0.145	95°	-0.409	0.128
(D-7) = (D-6)-(D-1)			0.375	6°	0.588	148°	0.196	100°	-0.020	0.161
D-8	~13 K	17:19:40 3-4-83 0.75 dia aperture	0.776	46°	0.367	114°	0.228	88°	-0.367	0.201
(D-9) = (D-8)-(D-1)			0.784	34°	0.343	127°	0.259	93°	+0.023	0.208
(D-10)	~13 K	Subtraction of 17:21:08 minus 17:19:40 of 3-4-83	0.377	140°	0.120	281°	0.198	59°	-0.223	0.099

FRED SUMMARY SHEET

DATE = 04/21/83 SERIAL : 987 USER : FRD TIME = 13/50/51

N.	DECK	FIT TYPE			SCALE	RMS	PK-PK	FOCUS	BLUR FOCUS	FOC.INCL. SPHERICAL	CYLINDER AMT.	CYLINDER ANG.	COMA AMT.	COMA ANG.	TRICORN AMT.	TRICORN ANG.	OR4
1	H83#1403	(SC)FOCUS			-0.50	0.212	1.631	-4.816									
1	H83#1403	(SC)ACT		OR4	-0.50	0.173	1.435	-4.156	-4.202	-4.740	0.092	79.	0.797	128.	0.187	89.	-0.584
2	H83#1401	(SC)FOCUS			-0.17	0.029	0.170	-C.200									
2	H83#1401	(SC)ACT		OR4	-0.17	0.017	0.098	-C.137	-0.208	-0.247	0.142	85.	0.177	47.	0.048	110.	-0.109
3	SUBTRACT	(SC)NONE	(G)		-0.17	0.206	1.559										
3	SUBTRACT	(SC)ACT	(G)	OR4	-0.17	0.151	1.349	C.687	0.642	0.072	0.091	39.	0.875	139.	0.215	88.	-0.615
4	H83#1391	(SC)FOCUS			-0.50	0.168	0.950	C.079									
4	H83#1391	(SC)ACT		OR4	-0.50	0.060	0.410	1.248	0.957	0.083	0.581	85.	0.060	153.	0.092	50.	-1.164
5	H83#1388	(SC)FOCUS			-0.17	0.037	0.221	C.509									
5	H83#1388	(SC)ACT	(G)	OR4	-0.17	0.020	0.146	-C.009	-0.036	-0.003	0.054	103.	0.106	66.	0.059	97.	0.006
6	SUBTRACT	(SC)NONE	(G)		-0.17	0.159	0.870										
6	SUBTRACT	(SC)ACT	(G)	OR4	-0.17	0.058	0.405	1.143	0.676	0.013	0.534	83.	0.124	216.	0.143	44.	-1.13C
6	SUBTRACT	(SC)NONE	(G)		-0.17	0.259	2.033										
6	SUBTRACT	(SC)ACT	(G)	OR4	-0.17	0.170	1.565	-C.456	-0.726	0.059	0.540	178.	0.855	131.	0.328	94.	0.515

THE TYPE OF OPD USED FOR EACH FIT WAS 'WAVEFRONT'
UNLESS DENOTED BY ONE OF THE FOLLOWING SYMBOLS:

(S) = SURFACE
(SP) = SINGLE PASS
(SC) = SCALED

(I) = INSERTED OR POLYNOMIAL
(M) = MIXED SURFACE/WAVEFRONT
(U) = USER-SPECIFIED TYPE

FITS DONE ON INTERPOLATED GRID ARE DENOTED BY (G).
ALL OTHER FITS ARE DONE ON MEASURED DATA.

ORIGINAL PAGE IS
OF POOR QUALITY

OSFRD887 OPTICSGO 13*53*08 83.111 PLOT NUMBER 6

SUBTRACT H83*1391 MINUS H83*1388

1

NONE (G) RMS 0.16 PKTPK 0.87 FRED SCALED

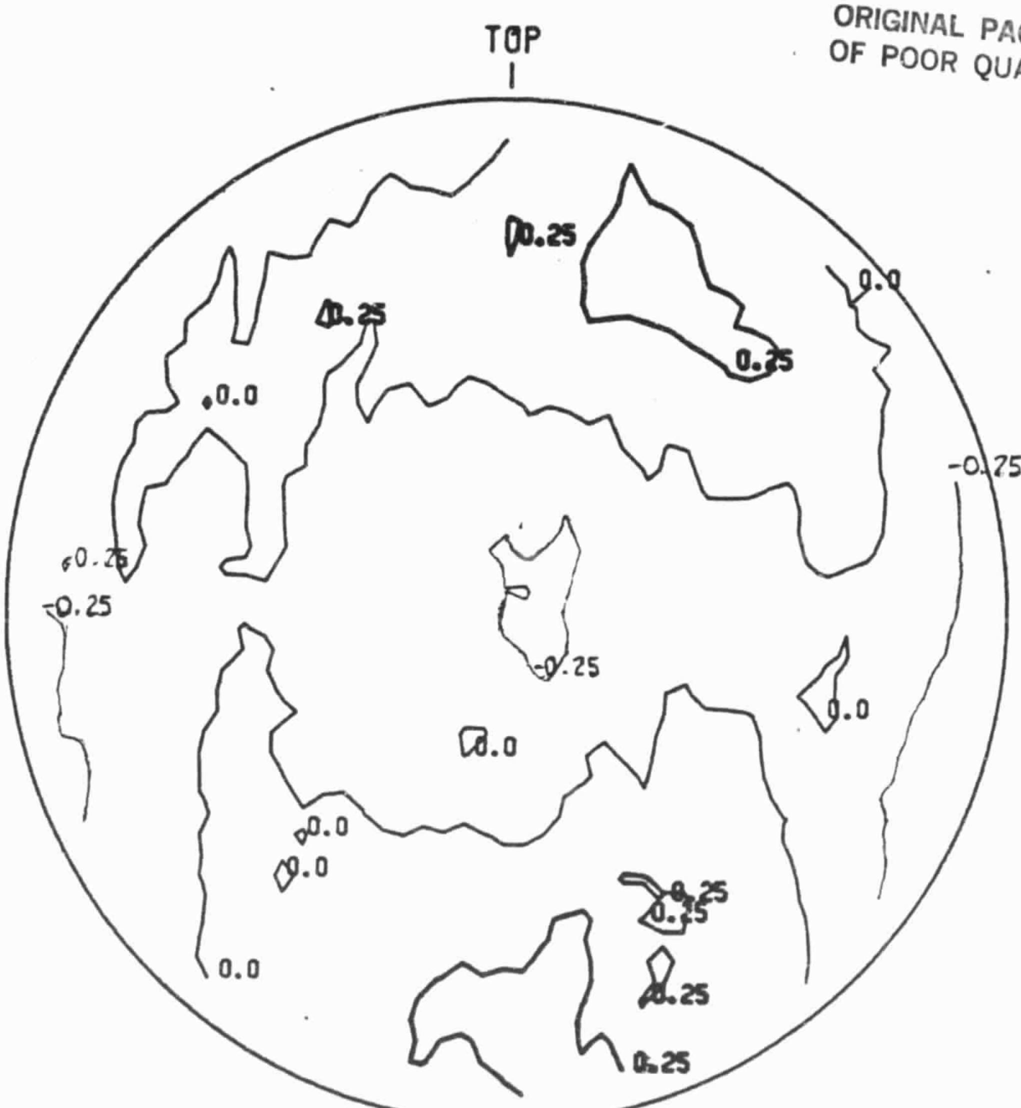

Figure D-1.Mirror Contour at Room Temperature
(Under Vacuum)

OSFRD887 OPTICSGO 13*52*28 83.111 PLOT NUMBER 3
SUBTRACT H83•1403 MINUS H83•1401
1
NONE (G) RMS 0.21 PKTPK 1.56 FRED SCALED

Figure D-2. Mirror Contour at 16:00 hrs., 3/4/83
(Mirror Temperature approx. 13 Kelvins)

JSFRD887 OPTICSGO 13*53*24 83.111 PLOT NUMBER 9

SUBTRACT SUBTRACT MINUS SUBTRACT

1

NONE (G) RMS 0.26 PKTPK 2.03 FRED SCALED

Figure D-3. Point-By-Point Subtraction
Figure D-2 minus Figure D-1

63

F R E D   S U M M A R Y   S H E E T

DATE = 04/21/83   SERIAL = 886
USER = FRD   TIME = 13/48/57

NO.	DECK	FIT TYPE			SCALE	RMS	PK-PK	FOCUS	BLUR FOCUS	FOC.INCL. SPHERICAL	CYLINDER AMT.	CYLINDER ANG.	COMA AMT.	COMA ANG.	TRICORN AMT.	TRICORN ANG.	DR4
1	CB3#0036	(SC)FOCUS			-0.50	0.292	1.849	-0.655									
1	CB3#0036	(SC)ACT		DR4	-0.50	0.139	1.220	-0.639	-1.151	-0.630	1.025	49.	0.949	117.	0.334	91.	0.008
2	HB3#1400	(SC)FOCUS			-0.17	0.035	0.188	-0.170									
2	HB3#1400	(SC)ACT		DR4	-0.17	0.019	0.104	-0.107	-0.161	-0.226	0.110	84.	0.223	45.	0.067	110.	-0.119
3	SUBTRACT	(SC)NONE	(G)		-0.17	0.277	1.704										
3	SUBTRACT	(SC)ACT	(G)	DR4	-0.17	0.136	1.020	-0.063	-0.551	0.050	0.974	49.	0.798	126.	0.273	90.	0.114
4	HB3#1391	(SC)FOCUS			-0.50	0.168	0.850	0.079									
4	HB3#1391	(SC)ACT		DR4	-0.50	0.060	0.410	1.248	0.957	0.083	0.581	85.	0.050	153.	0.092	50.	-1.164
5	HB3#1388	(SC)FOCUS			-0.17	0.037	0.221	0.509									
5	HB3#1388	(SC)ACT	(G)	DR4	-0.17	0.020	0.146	-0.009	-0.036	-0.003	0.054	103.	0.106	66.	0.059	97.	0.006
6	SUBTRACT	(SC)NONE	(G)		-0.17	0.159	0.870										
6	SUBTRACT	(SC)ACT	(G)	DR4	-0.17	0.058	0.405	1.143	0.876	0.013	0.534	83.	0.124	216.	0.143	44.	-1.130
6	SUBTRACT	(SC)NONE	(G)		-0.17	0.306	1.970										
6	SUBTRACT	(SC)ACT	(G)	DR4	-0.17	0.142	1.193	-1.206	-1.669	0.037	0.927	33.	0.806	117.	0.391	95.	1.243

THE TYPE OF OPD USED FOR EACH FIT WAS 'WAVEFRONT'
UNLESS DENOTED BY ONE OF THE FOLLOWING SYMBOLS:

(S) = SURFACE
(SP) = SINGLE PASS
(SC) = SCALED

(I) = INSERTED OR POLYNOMIAL
(M) = MIXED SURFACE/WAVEFRONT
(U) = USER-SPECIFIED TYPE

FITS DONE ON INTERPOLATED GRID ARE DENOTED BY (G).
ALL OTHER FITS ARE DONE ON MEASURED DATA.

ORIGINAL PAGE IS
OF POOR QUALITY

OSFRD886 OPTICSGO 13*50*31 83.111 PLOT NUMBER 3

SUBTRACT C83*0036 MINUS H83*1400

1

NONE (G) RMS 0.28 PKTPK 1.70 FRED SCALED

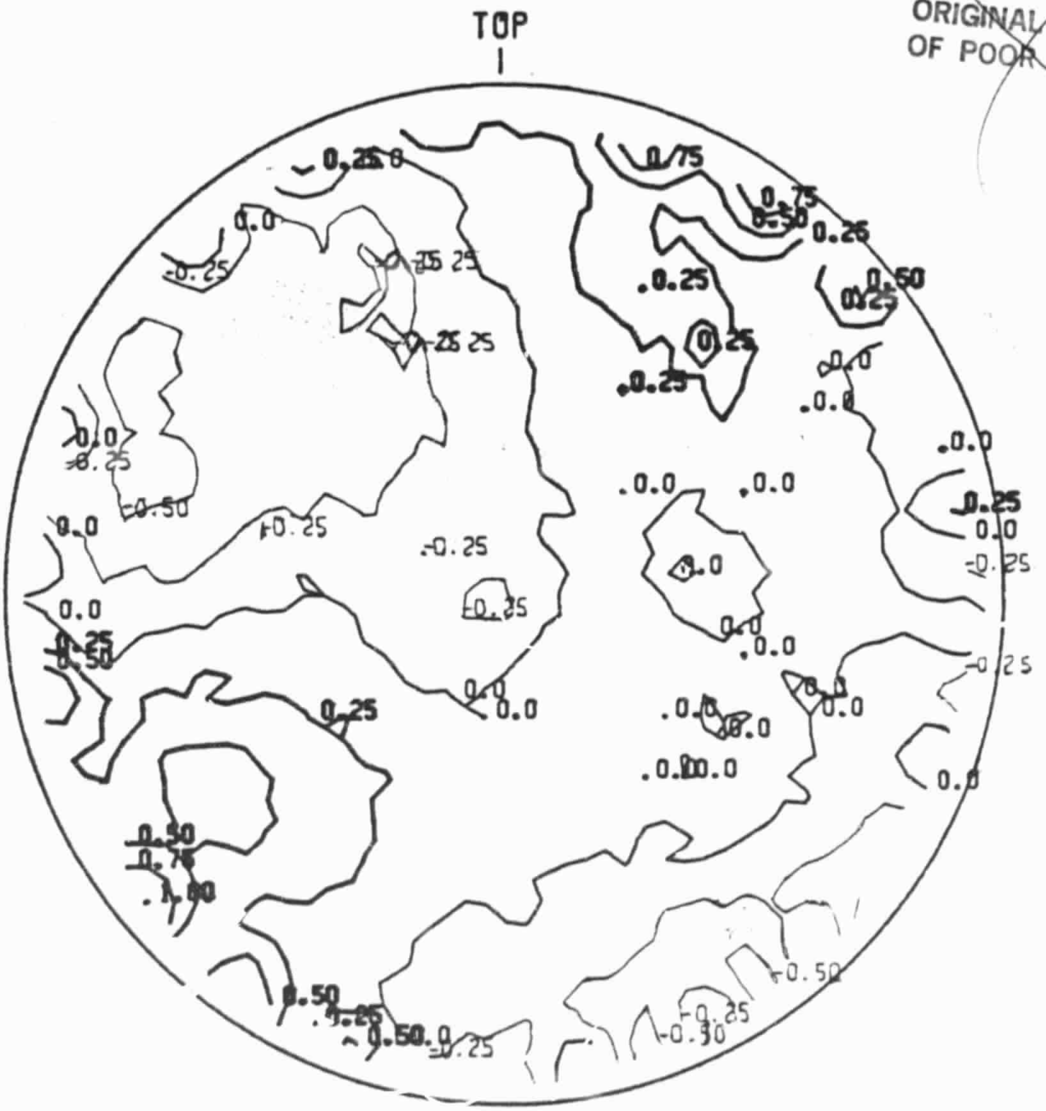

Figure D-4. Mirror Contour at 17:19:40 hrs., 3/4/83
(Mirror Temperature approx. 13 Kelvins)

OSFRD886 OPTICSGO 13*51*50 83.111 PLOT NUMBER 9

SUBTRACT SUBTRACT MINUS SUBTRACT

1

NONE (G) RMS 0.31 PKTPK 1.97 FRED SCALED

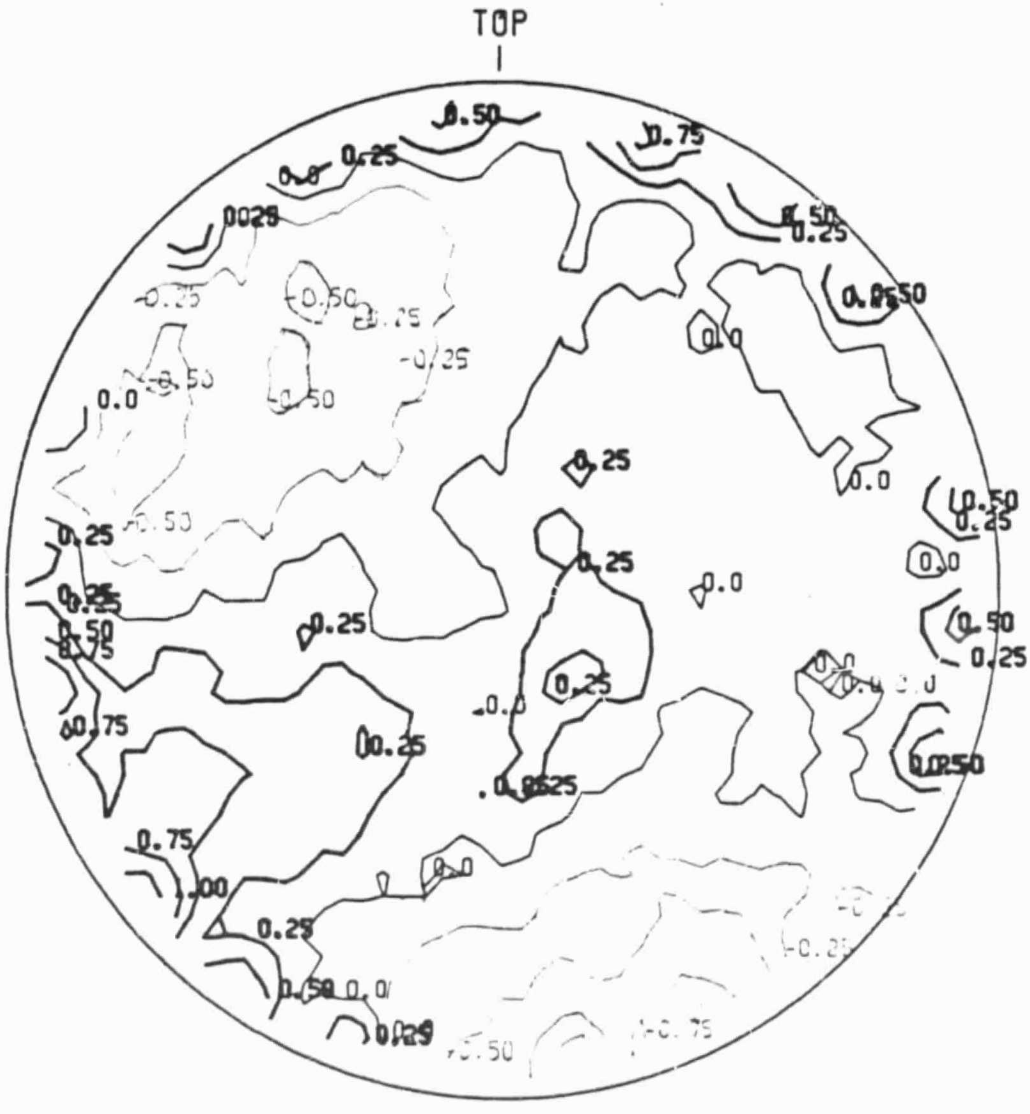

Figure D-5.Point-By-Point Subtraction Figure D-4 minus Figure D-1

FRED SUMMARY SHEET

DATE = 04/21/83 SERIAL = 988 USER = FRD TIME = 13/54/45 75% Aperture

NO.	DECK	FIT TYPE			SCALE	RMS	PK-PK	FOCUS	BLUR FOCUS	FOC.INCL. SPHERICAL	CYLINDER AMT.	CYLINDER ANG.	COMA AMT.	COMA ANG.	TRICORN AMT.	TRICORN ANG.	DR4
1	H83#1403	(SC)FOCUS			-0.50	0.133	0.944	-2.672									
1	H83#1403	(SC)ACT		DR4	-0.50	0.091	0.713	-2.215	-2.291	-2.577	0.152	46.	0.617	138.	0.117	97.	-0.361
2	H83#1401	(SC)FOCUS			-0.17	0.022	0.130	-0.091									
2	H83#1401	(SC)ACT		DR4	-0.17	0.014	0.074	-0.094	-0.142	-0.107	0.096	78.	0.054	69.	0.025	105.	-0.013
	SUBTRACT	(SC)NONE	(G)		-0.17	0.128	0.980										
	SUBTRACT	(SC)ACT	(G)	DR4	-0.17	0.080	0.599	0.509	0.445	0.100	0.128	34.	0.580	139.	0.145	95.	-0.405
	H83#1371	(SC)FOCUS			-0.50	0.099	0.515	0.370									
	H83#1371	(SC)ACT		DR4	-0.50	0.058	0.337	0.752	0.577	0.358	0.350	85.	0.114	71.	0.053	56.	-0.394
	H83#1398	(SC)FOCUS			-0.17	0.022	0.130	0.299									
	H83#1398	(SC)ACT	(G)	DR4	-0.17	0.010	0.098	-0.030	-0.045	-0.005	0.031	71.	0.059	122.	0.022	100.	0.025
	SUBTRACT	(SC)NONE	(G)		-0.17	0.094	0.531										
	SUBTRACT	(SC)ACT	(G)	DR4	-0.17	0.053	0.401	0.386	0.225	-0.003	0.322	86.	0.084	46.	0.068	51.	-0.389
	SUBTRACT	(SC)NONE	(G)		-0.17	0.161	1.046										
	SUBTRACT	(SC)ACT	(G)	DR4	-0.17	0.097	0.764	0.123	-0.065	0.103	0.375	6.	0.588	148.	0.196	100.	-0.020

THE TYPE OF OPD USED FOR EACH FIT WAS 'WAVEFRONT'
UNLESS DENOTED BY ONE OF THE FOLLOWING SYMBOLS:

(S) = SURFACE (I) = INSERTED OR POLYNOMIAL
(SP) = SINGLE PASS (M) = MIXED SURFACE/WAVEFRONT
(SC) = SCALED (U) = USER-SPECIFIED TYPE

FITS DONE ON INTERPOLATED GRID ARE DENOTED BY (G).
ALL OTHER FITS ARE DONE ON MEASURED DATA.

ORIGINAL PAGE IS
OF POOR QUALITY

OSFRD888 OPTICSGO 13*55*32 83.111 PLOT NUMBER 3
SUBTRACT H83*1403 MINUS H83*1401
1
NONE (G) RMS 0.13 PKTPK 0.88 FRED SCALED

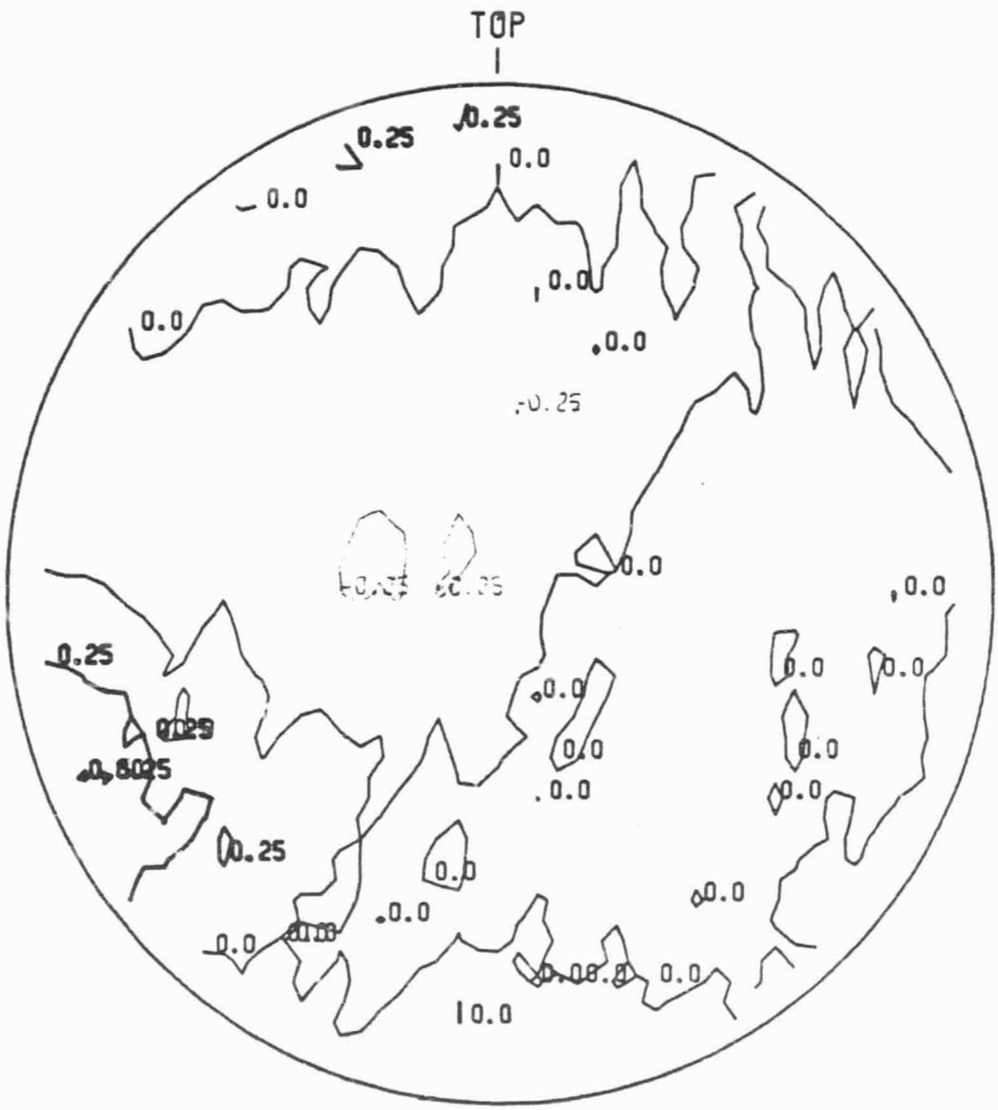

Figure D-6. 0.75 Diameter Aperture Mirror Contour
at 1600 hrs., 3/4/83

OSFRD888 OPTICSGO 13*56*07 83.111 PLOT NUMBER 9

SUBTRACT SUBTRACT MINUS SUBTRACT

1

NONE (G) RMS 0.16 PKTPK 1.05 FRED SCALED

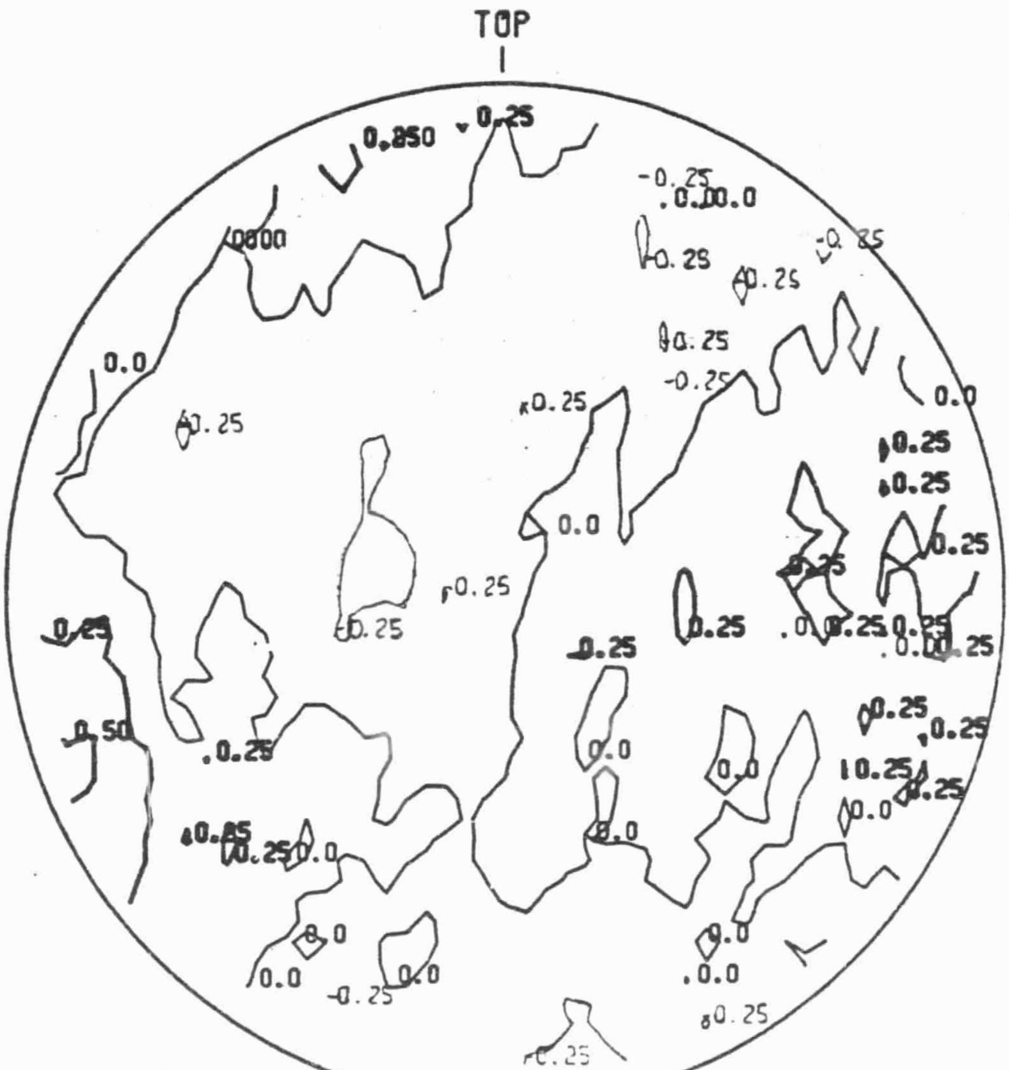

Figure D-7. 0.75 Diameter Point-By-Point Subtraction
Figure D-6 minus Figure D-1

F R E D   S U M M A R Y   S H E E T

75% APERTURE.

DATE = 04/21/83 SERIAL = 889 USER = FRD TIME = 13/57/02

NO.	DECK	FIT TYPE			SCALE	RMS	PK-PK	FOCUS	BLUR FOCUS	FOC.INCL. SPHERICAL	CYLINDER AMT.	CYLINDER ANG.	COMA AMT.	COMA ANG.	TRICORN AMT.	TRICORN ANG.	OR4
1	CA3#0036	(SC)FOCUS			-0.50	0.213	1.253	-0.326									
1	CA3#0036	(SC)ACT		OR4	-0.50	0.080	0.551	0.053	-0.355	-0.324	0.817	48.	0.416	111.	0.261	90.	-0.377
2	HA3#1400	(SC)FOCUS			-0.17	0.025	0.163	-0.088									
2	HA3#1400	(SC)ACT		OR4	-0.17	0.016	0.088	-0.060	-0.098	-0.092	0.074	76.	0.075	59.	0.039	103.	-0.032
3	SUBTRACT	(SC)NONE	(G)		-0.17	0.201	1.130										
3	SUBTRACT	(SC)ACT	(G)	OR4	-0.17	0.076	0.507	0.365	-0.024	-0.002	0.776	46.	0.367	114.	0.228	88.	-0.367
4	HA3#1391	(SC)FOCUS			-0.50	0.099	0.515	0.370									
4	HA3#1391	(SC)ACT		OR4	-0.50	0.058	0.367	0.752	0.577	0.358	0.350	85.	0.114	71.	0.053	56.	-0.394
5	HA3#1388	(SC)FOCUS			-0.17	0.022	0.130	0.289									
5	HA3#1388	(SC)ACT	(G)	OR4	-0.17	0.016	0.098	-0.030	-0.045	-0.005	0.031	71.	0.059	122.	0.022	100.	0.025
6	SUBTRACT	(SC)NONE	(G)		-0.17	0.094	0.531										
6	SUBTRACT	(SC)ACT	(G)	OR4	-0.17	0.053	0.431	0.386	0.225	-0.003	0.322	86.	0.084	49.	0.068	51.	-0.389
6	SUBTRACT	(SC)NONE	(G)		-0.17	0.208	1.328										
6	SUBTRACT	(SC)ACT	(G)	OR4	-0.17	0.086	0.567	-0.022	-0.414	0.001	0.784	34.	0.343	127.	0.259	93.	0.023

THE TYPE OF OPD USED FOR EACH FIT WAS 'WAVEFRONT'
UNLESS DENOTED BY ONE OF THE FOLLOWING SYMBOLS:

(S) = SURFACE
(SP) = SINGLE PASS
(SC) = SCALED

(I) = INSERTED OR POLYNOMIAL
(M) = MIXED SURFACE/WAVEFRONT
(U) = USER-SPECIFIED TYPE

FITS DONE ON INTERPOLATED GRID ARE DENOTED BY (G).
ALL OTHER FITS ARE DONE ON MEASURED DATA.

ORIGINAL PAGE IS
OF POOR QUALITY

OSFAD889 OPTICSGO 13*57*57 83.111 PLOT NUMBER 3

SUBTRACT C83*0036 MINUS H83*1400 75%

1

NONE (G) RMS 0.20 PKTPK 1.13 FRED SCALED

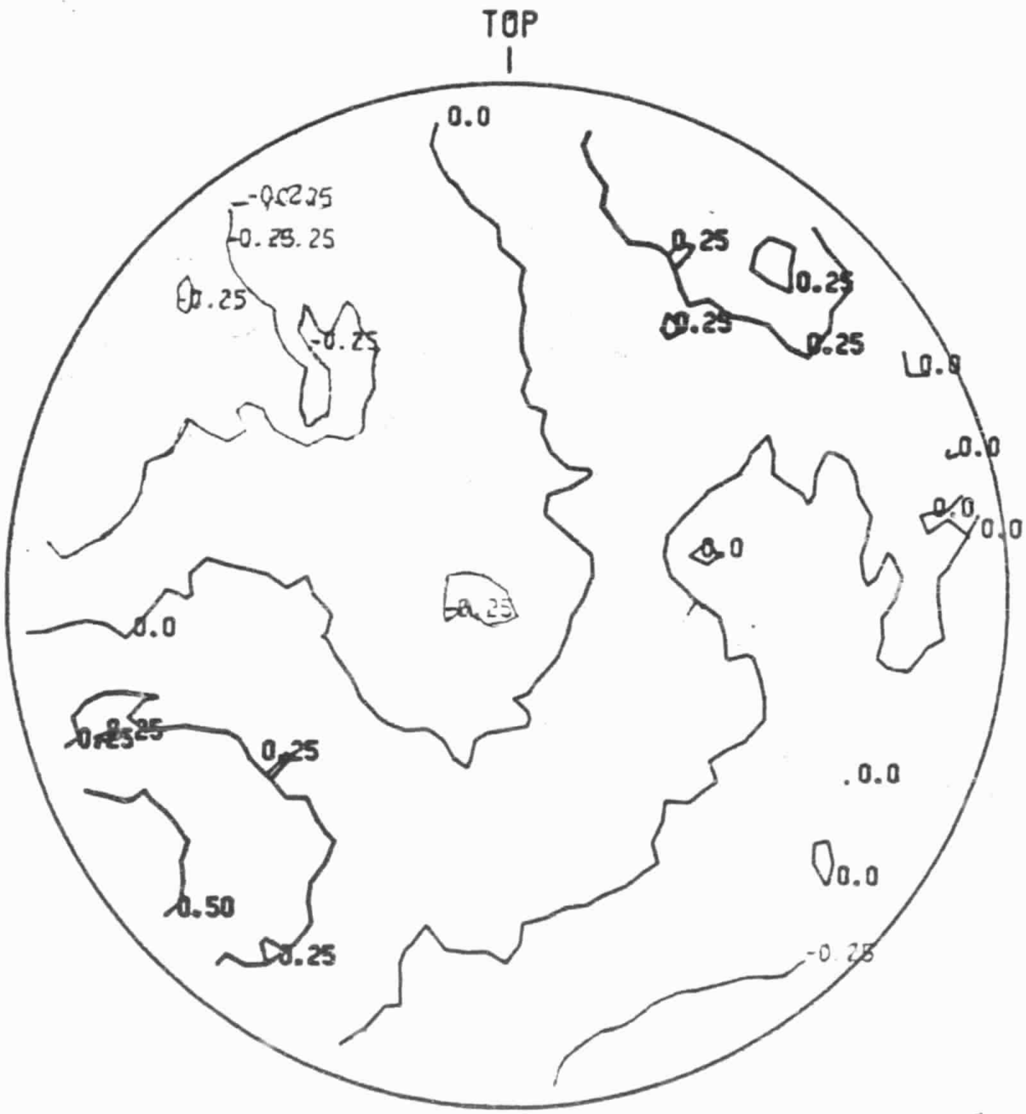

Figure D-8. 0.75 Diameter Aperture
Mirror Contour at 17:19:40, 3/4/83

OSFRD889 OPTICSGO 13*58*39 83.111 PLOT NUMBER 9

SUBTRACT SUBTRACT MINUS SUBTRACT

1

NONE (G) RMS 0.21 PKTPK 1.33 FRED SCALED

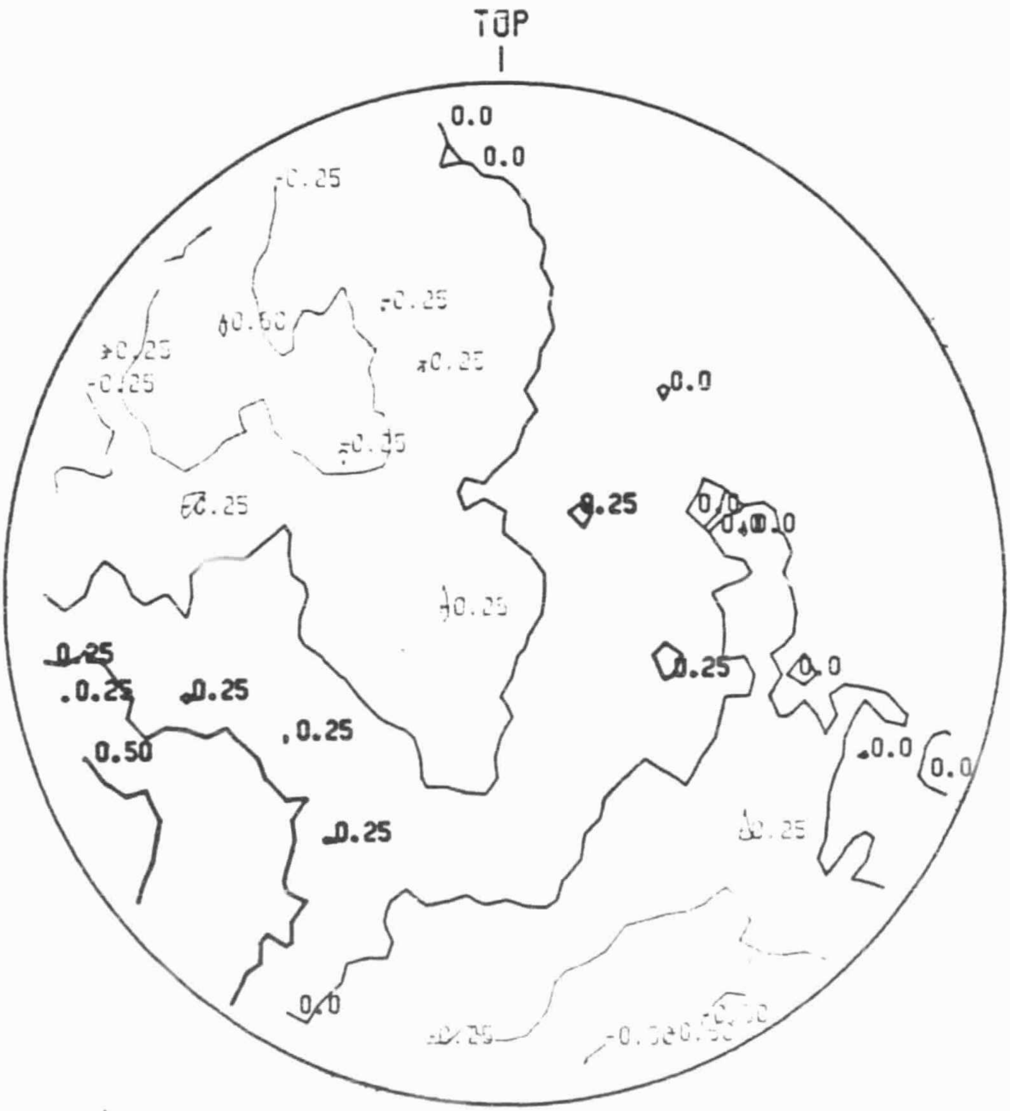

Figure D-9.0.75 Diameter Point-By-Point Subtraction of Figure D-8 minus Figure D-1

F R E D   S U M M A R Y   S H E E T

DATE = 05/10/83   SERIAL = 058   TIME = 9/56/25
USER = FRD

NO.	DECK	FIT TYPE			SCALE	RMS	PK-PK	FOCUS	BLUR FOCUS	FOC.INCL. SPHERICAL	CYLINDER AMT.	CYLINDER ANG.	COMA AMT.	COMA ANG.	TRICORN AMT.	TRICORN ANG.	OR4
1	C83#0093	(SC)FOCUS			-0.50	0.235	1.770	-0.664									
1	C83#0093	(SC)ACT		OR4	-0.50	0.120	1.120	-0.457	-0.838	-0.713	0.763	47.	0.856	121.	0.368	82.	-0.256
2	C83#0036	(SC)FOCUS			-0.50	0.292	1.849	-0.655									
2	C83#0036	(SC)ACT		OR4	-0.50	0.139	1.220	-0.639	-1.151	-0.630	1.025	49.	0.949	117.	0.334	91.	0.008
3	SUBTRACT	(SC)NONE	(G)		-0.50	0.147	1.776										
3	SUBTRACT	(SC)ACT	(G)	OR4	-0.50	0.099	1.231	0.163	-0.026	-0.060	0.377	140.	0.120	281.	0.198	59.	-0.223
3	SUBTRACT	(SC)ACT	(G)	OR4	-0.50	0.099	1.231	0.000	0.000	-0.000	0.000	0.	0.000	0.	0.000	0.	-0.000

THE TYPE OF OPD USED FOR EACH FIT HAS 'WAVEFRONT'
UNLESS DENOTED BY ONE OF THE FOLLOWING SYMBOLS:

(S) = SURFACE   (I) = INSERTED OR POLYNOMIAL
(SP) = SINGLE PASS   (M) = MIXED SURFACE/WAVEFRONT
(SC) = SCALED   (U) = USER-SPECIFIED TYPE

FITS DONE ON INTERPOLATED GRID ARE DENOTED BY (G).
ALL OTHER FITS ARE DONE ON MEASURED DATA.

POLYNOMIAL EQUATION USED FOR STANDARD FITS

$$W = A + BX + CY + DR^2 + E(X^2 - Y^2) + FXY$$
$$+ GXR^2 + HYR^2 + I(X^3 - 3XY^2) + J(-Y^3 + 3X^2Y)$$
$$+ KR^4 + LR^6 + MR^8 + NR^{10}$$

ABERRATION ANGLE CONVENTION
POSITIVE ANGLE TO FIRST MAXIMUM AT EDGE

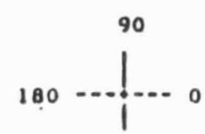

[illegible] 09-59-22 83.130 PLOT NUMBER 4

SUBTRACT C83=0093 MINUS C83=0036

1

NONE (G) RMS 0.15 PKTPK 1.78 FRED SCALED

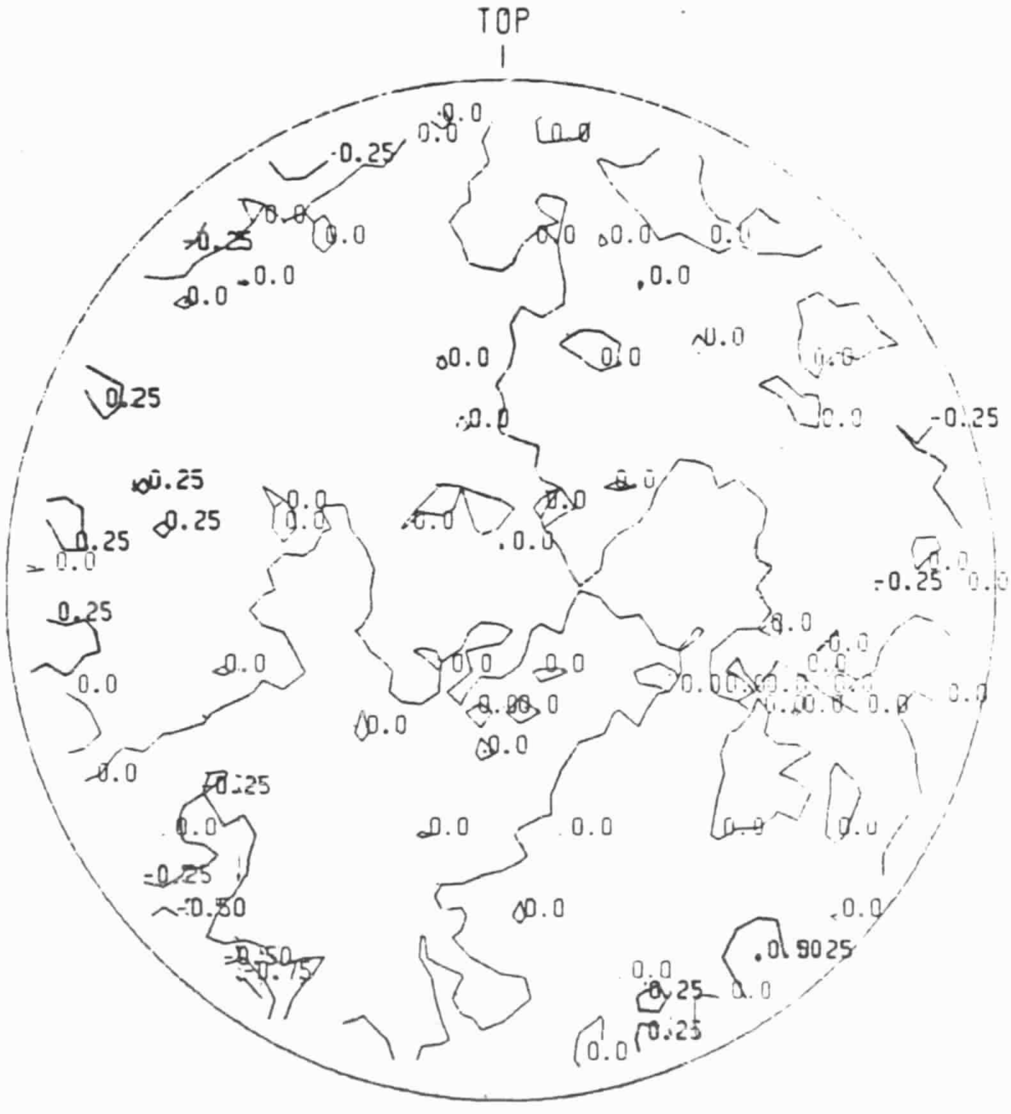

Figure D-10. Full Aperture Point-By-Point Subtraction of Mirror Contour at 17:21:08 minus Contour at 17:19:40 on 3/4/83

APPENDIX E

INTERFEROMETRIC DATA REDUCTION - SECOND COLD CYCLE

The only interferometric data reduced for the second cold test cycle is shown on the FRED summary sheet, serial #681. Deck No. H831751 is for the interferogram (Polaroid) taken at 8:56:05 on 5/19/83 with the mirror at approximately 15 Kelvins. Window aberrations, again verified as small, were not subtracted. Deck No. H831750 is for the interferogram taken on 5/23/83, at which time the thermocouple data record indicates that the mirror temperature was changing less than 0.2K per hour. Contour plot figure numbers are indicated on page 2 of the summary.

Note that FRED data have not been scaled and thus represent wavefront values. Multiplying by -0.5 to obtain mirror surface deflections, one finds that the values are comparable to those of the first cold cycle.

The temperature-time plots of Figures E-9 and E-10 appear self-explanatory.

```
*****************************************
*   F R E D    S U M M A R Y    S H E E T   *
*****************************************
```

DATE = 07/15/83 SERIAL # 681 USER # FRD TIME = 11/24/13

NO.	DECK	FIT TYPE	SCALE	RMS	PK-PK	FOCUS	BLUR FOCUS	FOC.INCL. SPHERICAL	CYLINDER AMT.	CYLINDER ANG.	COMA AMT.	COMA ANG.	TRICORN AMT.	TRICORN ANG.	DR4
1	H8301750	FOCUS		0.987	1.827	0.190									
1	H8301750	ACT (G) DR4		0.110	0.711	2.275	1.487	0.144	1.577	79.	0.189	131.	0.165	61.	-2.131
2	H8301751	FOCUS		0.517	3.016	1.029									
2	H8301751	ACT (G) DR4		0.248	1.988	-1.517	-2.029	-0.229	1.024	133.	1.823	291.	0.572	21.	1.288

THE TYPE OF OPD USED FOR EACH FIT HAS 'WAVEFRONT'
UNLESS DENOTED BY ONE OF THE FOLLOWING SYMBOLS:

(S) = SURFACE
(SP) = SINGLE PASS
(SC) = SCALED
(I) = INSERTED OR POLYNOMIAL
(M) = MIXED SURFACE/WAVEFRONT
(U) = USER-SPECIFIED TYPE

FITS DONE ON INTERPOLATED GRID ARE DENOTED BY (G).
ALL OTHER FITS ARE DONE ON MEASURED DATA.

POLYNOMIAL EQUATION USED FOR STANDARD FITS:

$$W = 1 + FX + CY + DR^2 + E(X^2-Y^2) + FXY + GXR^2 + HYR^2 + I(X^3-3XY^2) + J(-Y^3+3X^2Y) + KR^4 + LR^6 + MR^8 + NR^{10}$$

ABERRATION ANGLE CONVENTION:
POSITIVE ANGLE TO FIRST MAXIMUM AT EDGE

```
        90
        |
180 ----+---- 0
        |
       270
```

ORIGINAL PAGE IS
OF POOR QUALITY

```
    * REMP ROS : CFRD : LIB : 08454ONE
    * FRED
-INC HE3#1750
* THE CARD(S) SPECIFIED ABOVE HAVE BEEN PLACED IN THE JOB STREAM
    SCALE FID CIPC
    APERTURE CAC 1.001
    FIT FOCUS
    GRID 31 31
    MAP GRID FULL                    FIGURE No.
    PLOT -2. 2. 0.1 NO LAB             E-1
    PLOT -2. 2. 0.25                   E-2
    FIT ACT OR4 GRID
    PLOT -2. 2. 0.1 NO LAB             E-3
    PLOT -2. 2. 0.25                   E-4
-INC HE3#1751
* THE CARD(S) SPECIFIED ABOVE HAVE BEEN PLACED IN THE JOB STREAM
    SCALE FID CIPC
    APERTURE CAC 1.001
    FIT FOCUS
    GRID 31 31
    MAP GRID FULL
    PLOT -2. 2. 0.1 NO LAB           E-5
    PLOT -2. 2. 0.25                 E-6
    FIT ACT OR4 GRID
    PLOT -2. 2. 0.1 NO LAB           E-7
    PLOT -2. 2. 0.25                 E-8
```

OSFRD681 OPTICSGO 11*24*33 83.196 PLOT NUMBER 1

H83*1750 8454 STITF 7/25/83

TONY DEFRANZO 7/15/8?

FOCUS RMS 0.39 PKTPK 1.83 FRED WAVEFRONT

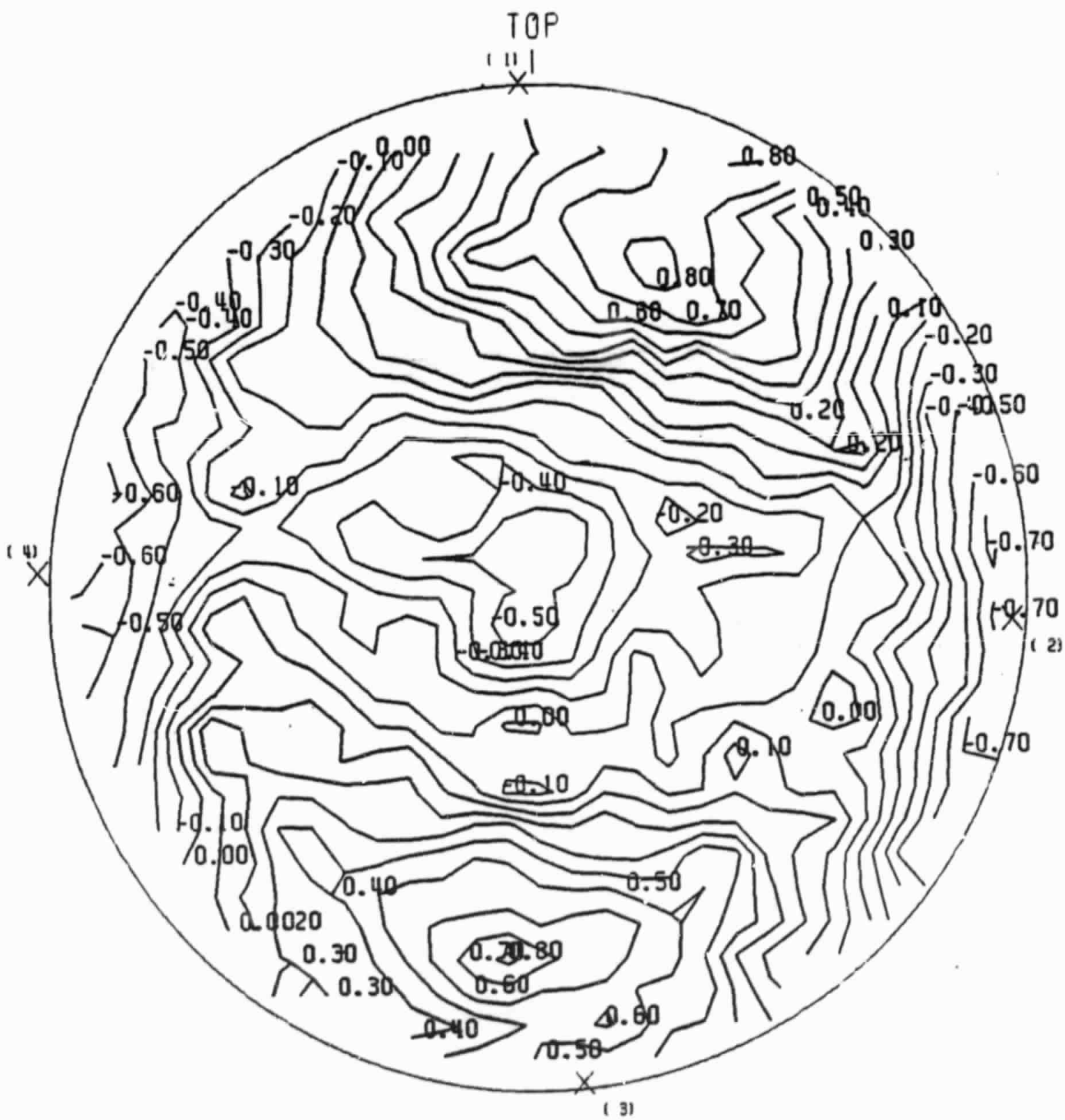

Figure E-1

OSFRD681 OPTICSGO 11*24*34 83.196 PLOT NUMBER 2

H83*1750 8454 STITF 7/25/83

TONY DEFRANZO 7/15/83

FOCUS RMS 0.39 PKTPK 1.83 FRED WAVEFRONT

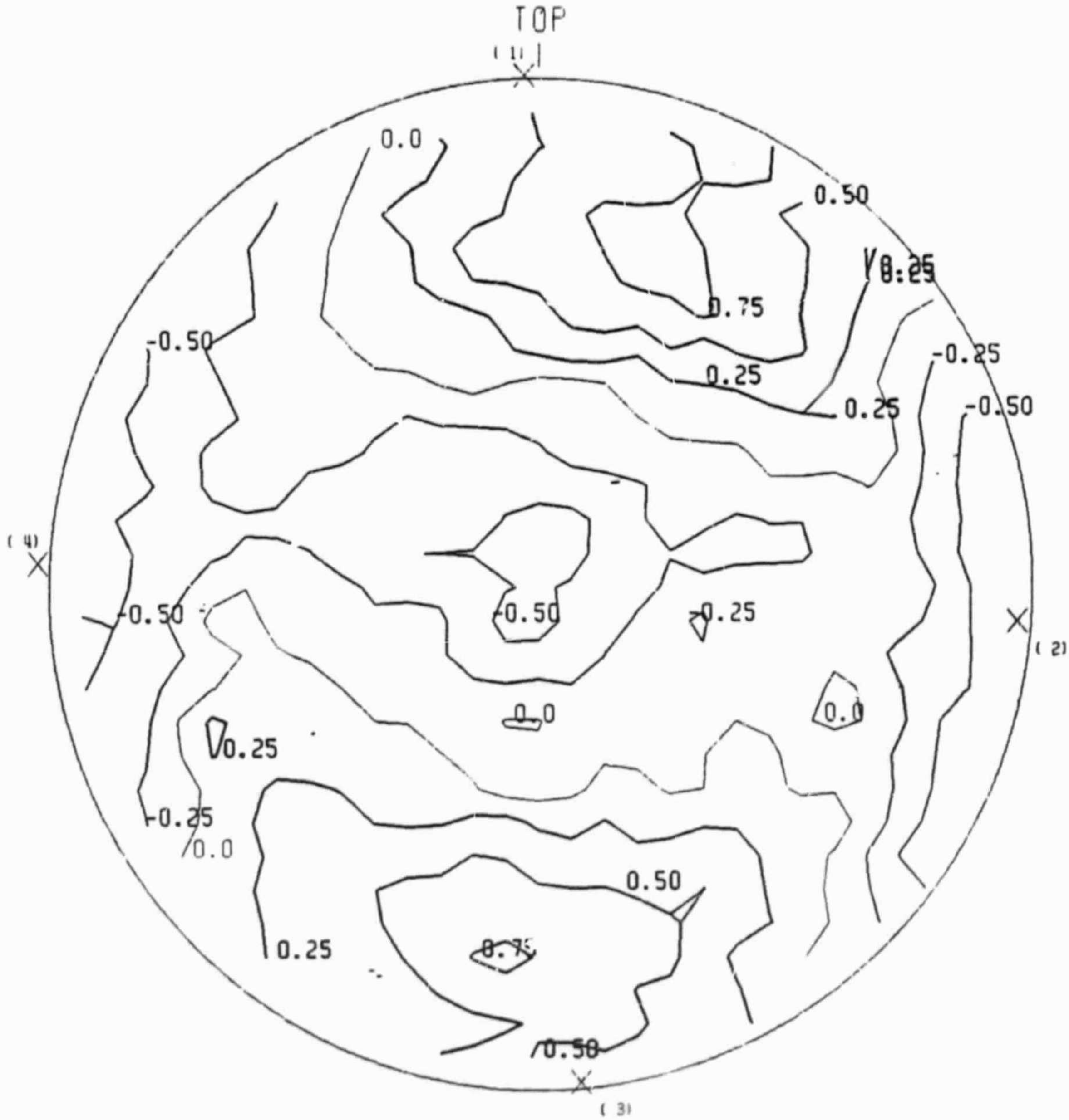

Figure E-2

OSFRD681 OPTICSGO 11*24*35 83.196

H83#1750 8454 STIIF 7/25/83

TONY DEFRANZO 7/15/83

ACT (G) OR4 RMS 0.11 PKTPK 0.71 FRED WAVEFRONT

PLOT NUMBER 3

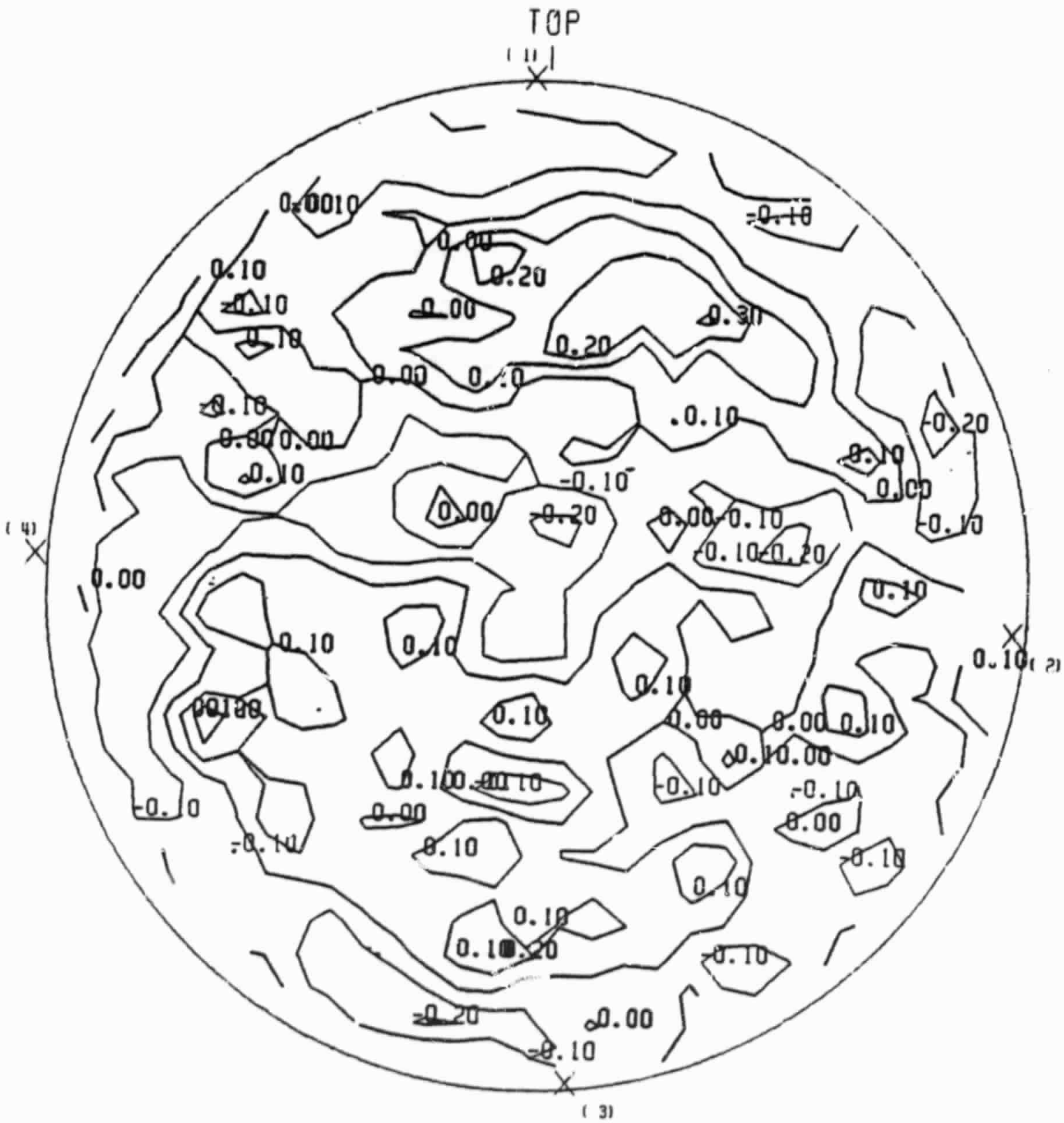

Figure E-3

OSFRD681 OPTICSGO 11*24*37 83.196 PLOT NUMBER 4

H83*1750 8454 STITF 7/25/83

TONY DEFRANZO 7/15/83

ACT (G) OR4 RMS 0.11 PKTPK 0.71 FRED WAVEFRONT

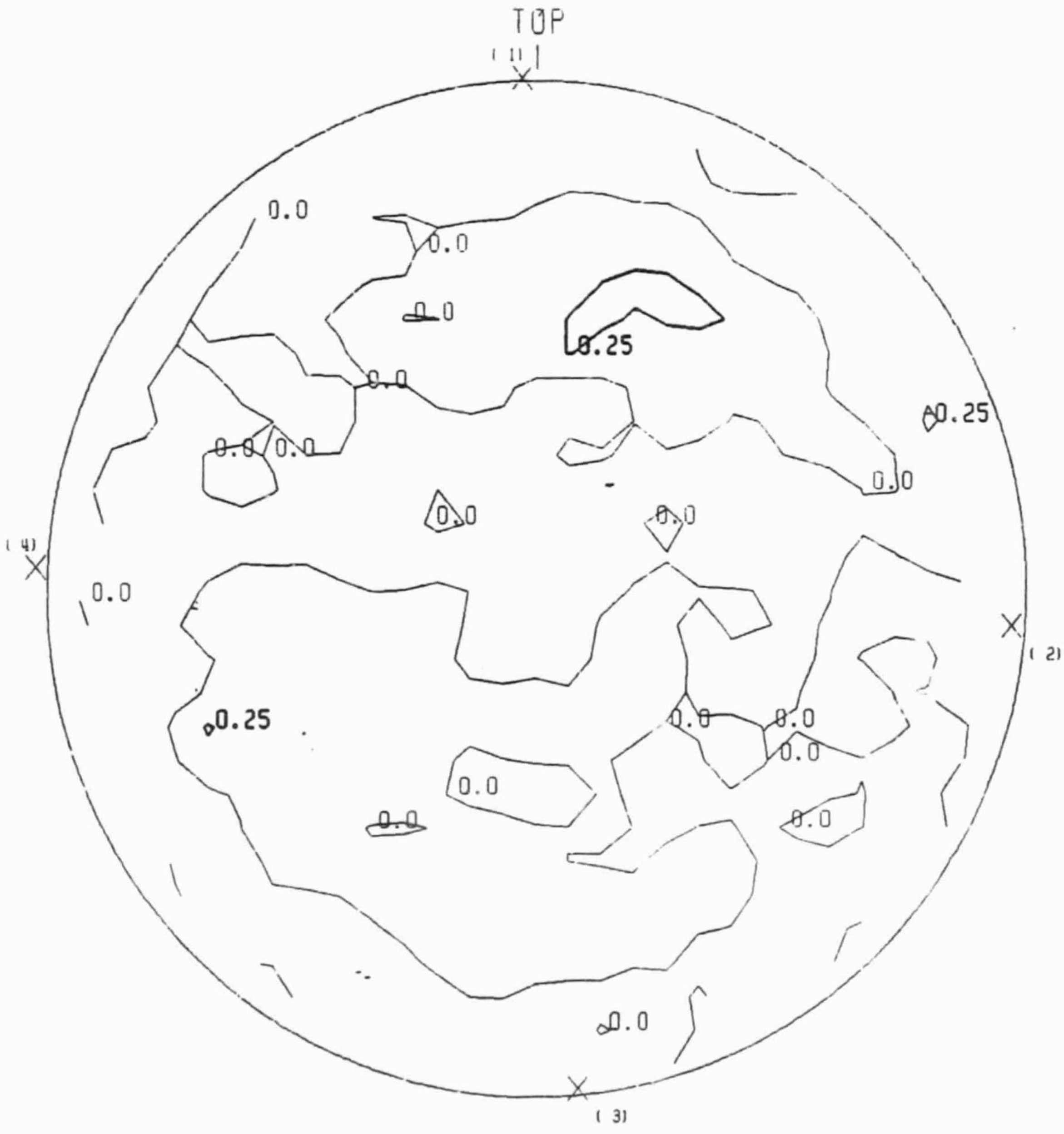

Figure E-4

OSFRD681 OPTICSGO 11*24*52 83.196 PLOT NUMBER 5
H83*1751 8454.BA SIRTF 14K 5/19/83
D MANSUR 7/15/83 AM
FOCUS RMS 0.52 PKTPK 3.02 FRED WAVEFRONT

ORIGINAL PAGE IS
OF POOR QUALITY

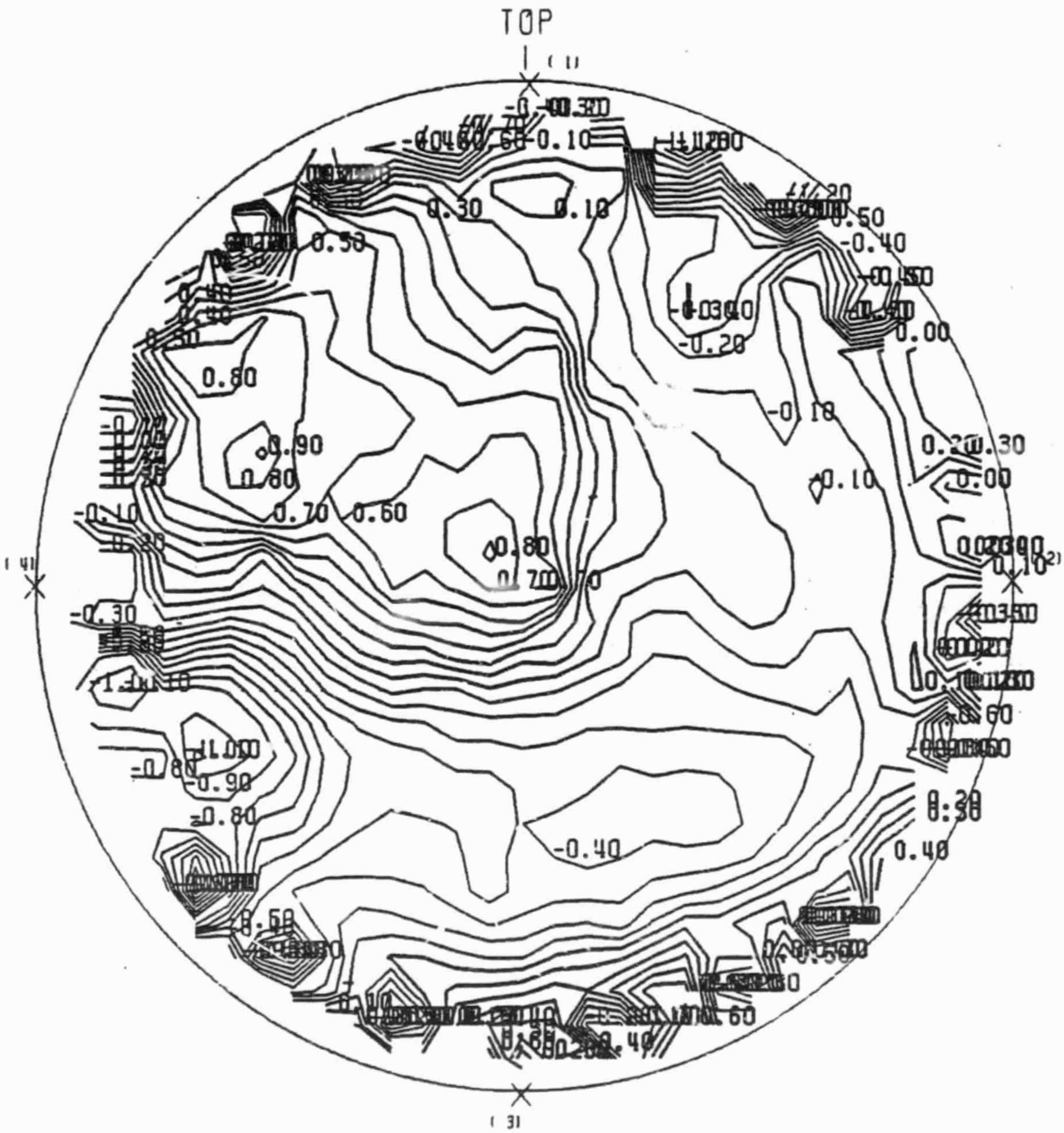

Figure E-5

OSFRD681 OPTICSGO 11*24*53 83.196

H83*1751 8454.BA SIRTF 14K 5/19/83 PLOT NUMBER 6

D MANSUR 7/15/83 AM

FOCUS RMS 0.52 PKTEK 3.02 FRED WAVEFRONT

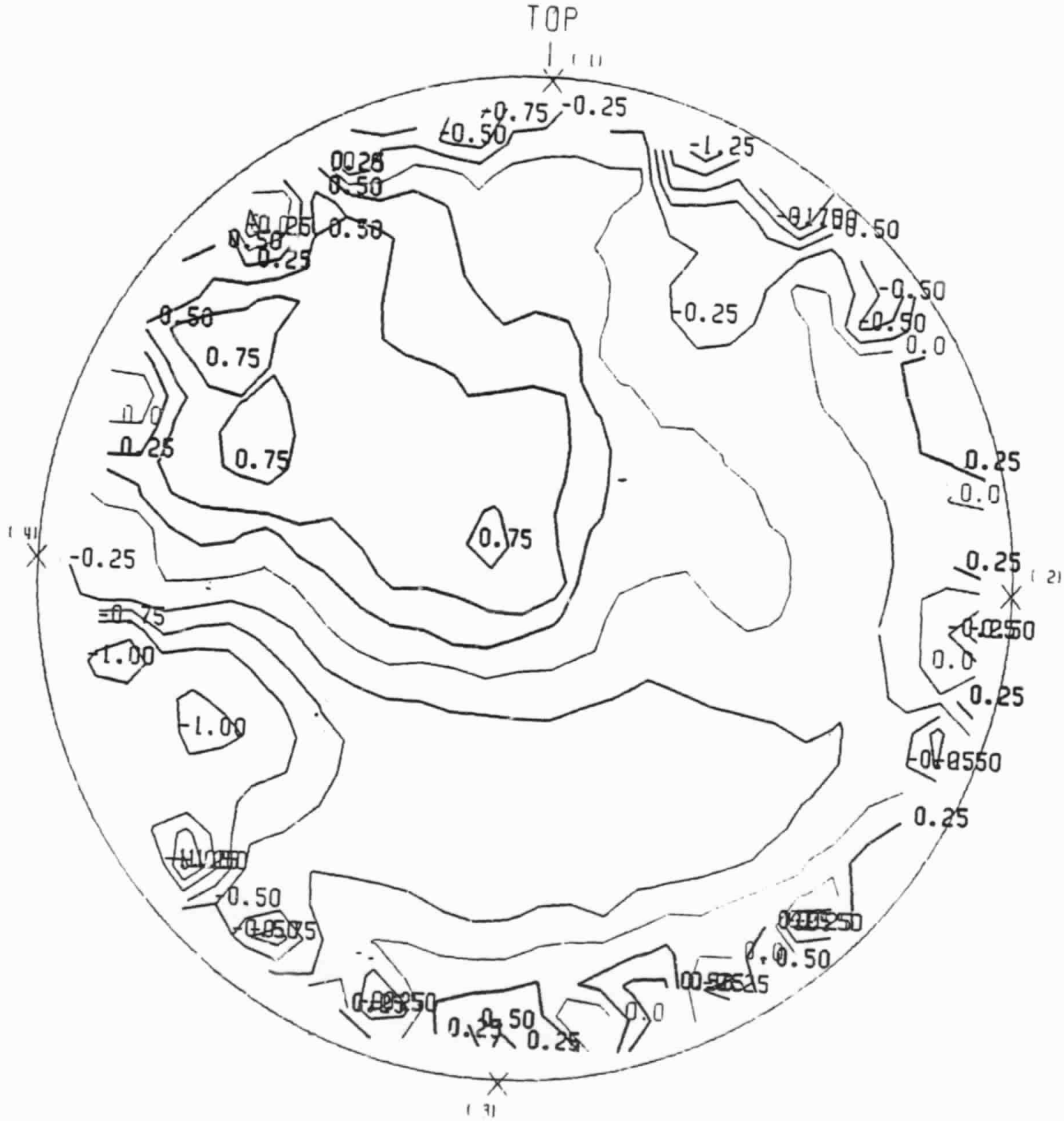

Figure E-6

OSFRD681 OFTICSGO 11*24*54 83.196 PLOT NUMBER 7

H83*1751 8454.BA SIRTF 14K 5/19/83

D MANSUR 7/15/83 AM

ACT (G) OR4 RMS 0.25 PKTPK 1.99 FRED WAVEFRONT

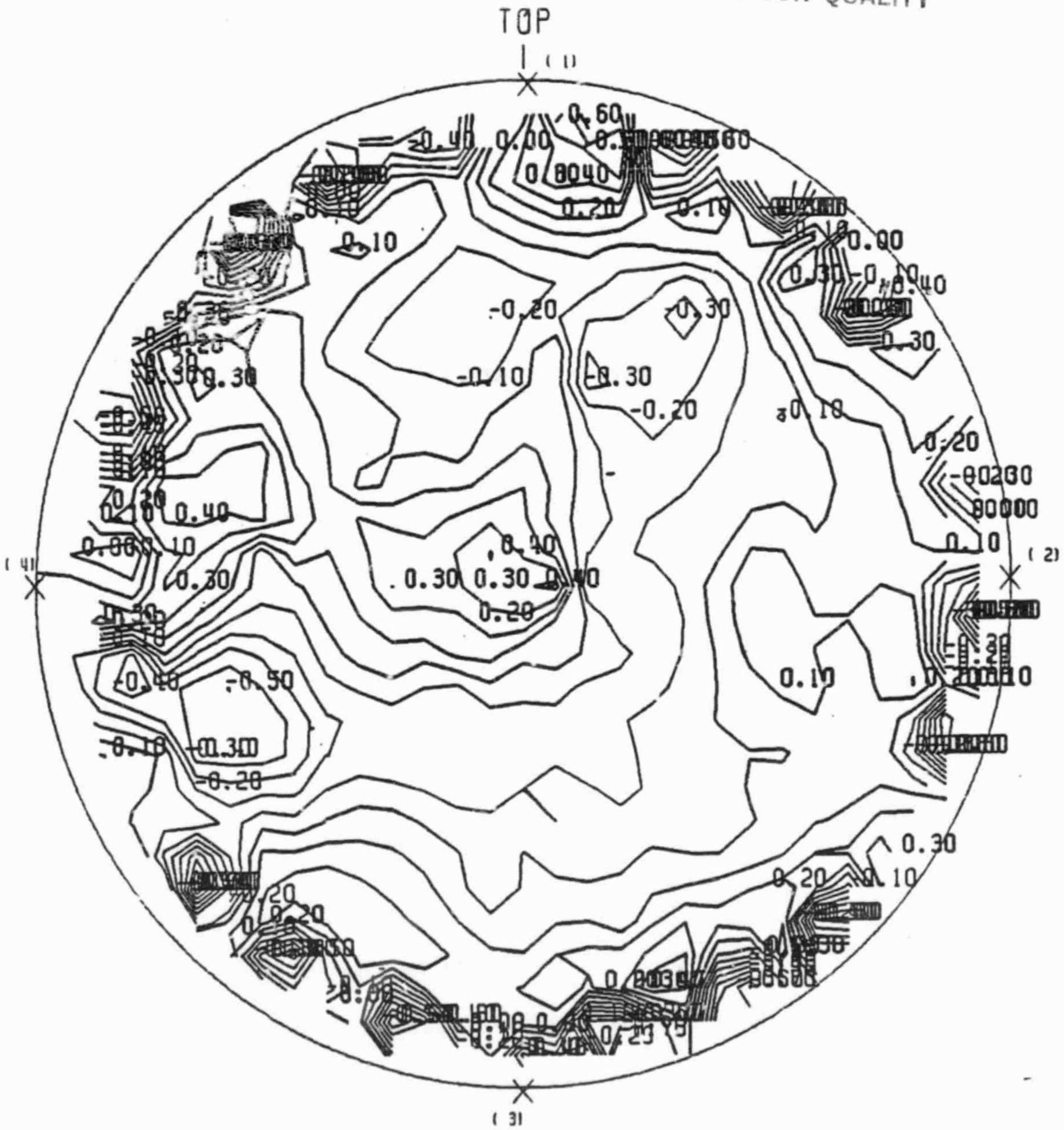

Figure E-7

OSFRD681 OPTICSGO 11*24*55 83.196

H83*1751 8454.8A SIATF 14K 5/19/83 PLOT NUMBER 8

D MANSUR 7/15/83 AM

ACT (G) 0A4 RMS 0.25 PKTPK 1.99 FRED WAVEFRONT

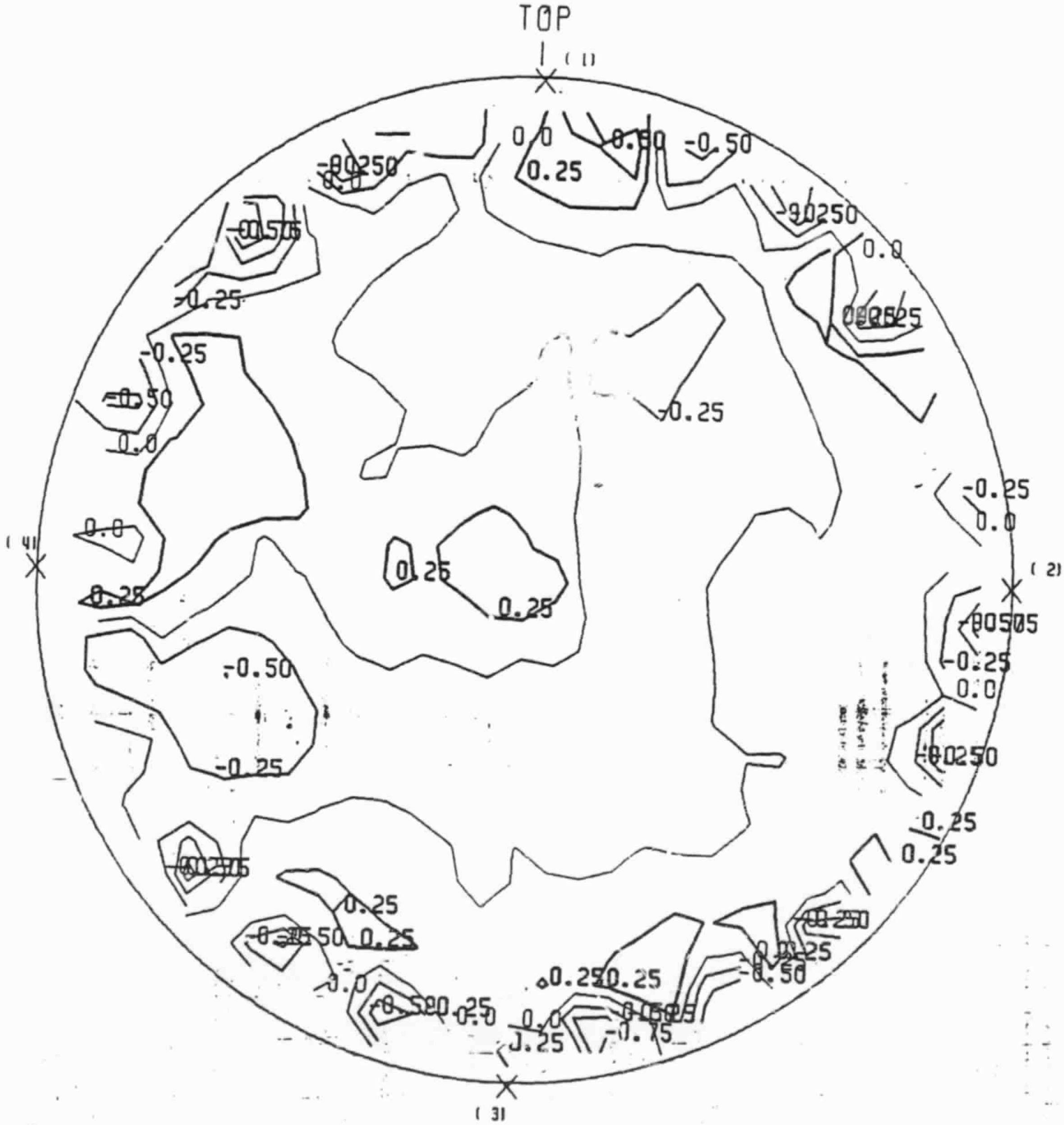

Figure E-8

BY:		TITLE: Mirror Temperatures 08:30 - 09:30 hrs., 5/19/83	PAGE:
DEPT:	DATE:		PROJECT:

Curve	Diode	Location on Mirror
①	D4866	Rear, Center
②	D4948	Rear, 6 o'clock, near edge
③	D4781	Rear, 9 o'clock, near edge
④	D3880	Mid-side, 3 o'clock

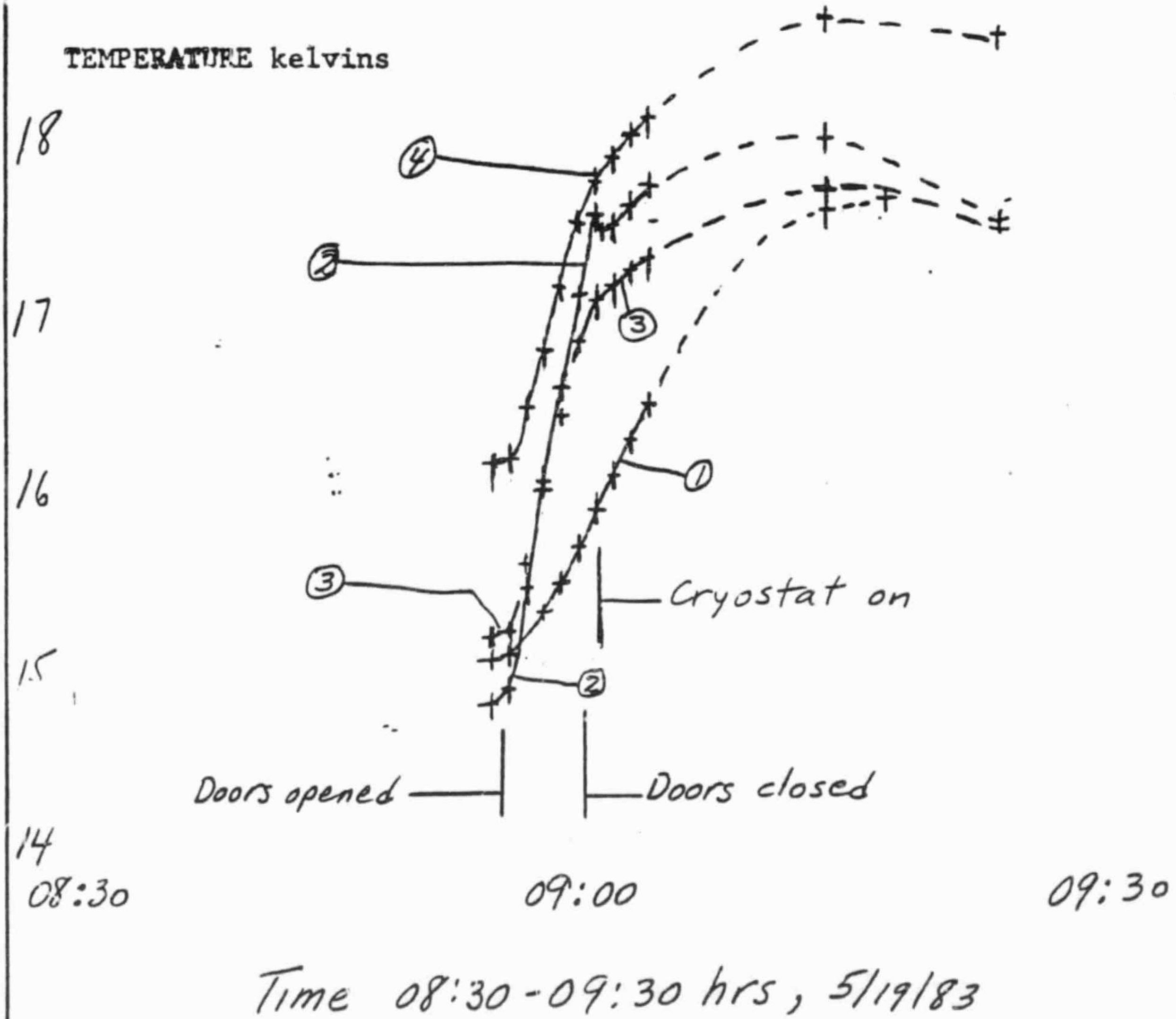

FIGURE E-9

E 103 REL 8/66 ENGINEERING ANALYSIS SHEET

BY:		TITLE: Mirror and Shroud Temps. during video runs	PAGE:
DEPT:	DATE:		PROJECT:

FIGURE E-10